

Universidade Federal de Minas Gerais – UFMG

Instituto de Ciências Exatas – ICEx

Departamento de Química

Daniel Lippross

**Production and characterisation of two-
dimensional molybdenum disulphide by exfoliation for innovative
applications**

BELO HORIZONTE

2019

UFMG/ICEx/DQ. 1350^a

D. 734^a

Daniel Lippross

Production and characterisation of two-dimensional molybdenum disulphide by exfoliation for innovative applications.

Dissertação apresentada ao Departamento de Química do Instituto de Ciências Exatas da Universidade Federal de Minas Gerais como requisito parcial para a obtenção do grau de Mestre em Química – Físico-Química.

Ficha Catalográfica

L765p Lippross, Daniel Edward
2019 Production and characterisation of two-dimensional
D molybdenum disulphide by exfoliation for innovative
applications [manuscrito] /Daniel Lippross
60 f.: il.

Orientadora: Glaura Goulart Silva

Dissertação (mestrado) - Universidade Federal de
Minas Gerais - Departamento de Química.
Inclui bibliografia.

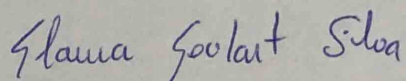
1. Físico química - Teses 2. Microscopia de força
atômica - Teses 3. Microscopia eletrônica de
varredura - Teses 4. Raman, Espectroscopia de - Teses
5. Capacitores- Teses 6. Grafeno- Teses I. Silva,
Glaura Goulart - Orientadora II. Título

CDU 043

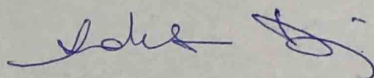
**"Production and Characterisation of Two-Dimensional Molybdenum Disulphide
by Exfoliation for Innovative Applications"**

Daniel Edward Lippross

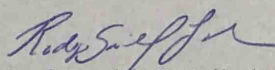
Dissertação aprovada pela banca examinadora constituída pelos Professores:



Profa. Glaura Goulart Silva - Orientadora
UFMG



Prof. Anderson Dias
UFMG



Prof. Rodrigo Gribel Lacerda
UFMG

Belo Horizonte, 04 de julho de 2019.

Este trabalho foi desenvolvido no Laboratório de Materiais Poliméricos do Departamento de Química da Universidade Federal de Minas Gerais sob a orientação da Professora Dra. Glaura Goulart Silva.

Acknowledgements:

I would like to first thank Petrobras for the financial resources in making this project possible.

To CAPES for providing me with a bursary for study.

I would like to thank Professor Glaura Goulart Silva, for all the guidance, support and belief in me. You have given me an opportunity I will never forget, and I hope I shall always do you proud.

To Professor Rodrigo Lassarote Lavall, thank you for your guidance in working with supercapacitors. You are a great inspiration.

To Dr. Thiago Cunha, thank you for working with me in making a gas sensor device. I always enjoyed our conversations.

To my colleagues in the Grupo de Materiais Poliméricos Multicomponentes for your undying support and friendship. In particular, I would like to thank Felipe da Silva Medeiros, Alan Sakita, Jesus Nuncira Valencia. You are all in my eyes as scientists second to none.

To my colleagues at CTnano, for your support and friendship. Your company will grow great through your tremendous efforts, I feel proud to have been even a small part of this.

To my colleagues in the Centro de Microscopia da UFMG. Thank you for performing the measurements of SEM, TEM and AFM. I will always respect your professionalism.

To my parents Angela and Martin, your unconditional love, words of encouragement and belief in me my whole life are the foundation of who I am.

To my brother George for all your support and friendship.

To all my friends in particular Billy, Jack and Oliver. You have all been with me for many years and your support and friendship always drive me forward.

To the professors of the department of chemistry at UFMG.

Table of Contents

Figures	6
Tables	8
List of abbreviations	9
1. Abstract	10
1.1 Português	11
3.2 English.....	12
2. Introduction	13
3. Literature review	15
3.1 Two-dimensional MoS ₂	15
3.2 Preparation of MoS ₂	17
3.3 Characterization of MoS ₂	21
3.4 Applications of MoS ₂	24
3.4.1 Supercapacitors	25
3.4.2 Humidity Sensors	27
4. Objectives	29
5. Methodologies	30
6. Results and Discussion	35
7. Conclusions	52
8. References	53

Figures

Figure. 1 3D ball and stick model of 2H-MoS ₂	15
Figure. 2 A) Ligand field splitting for trigonal prismatic MoS ₂ and B) octahedral MoS ₂	17
Figure. 3 An overview of the exfoliation process of MoS ₂	18
Figure. 4 Pathway of phase transitions for MoS ₂	20
Figure. 5 Galvanostatic discharge curve for Li intercalation of MoS ₂	21
Figure. 6 AFM cantilever and sample system	22
Figure. 7 Ragone plot of energy storage devices.....	24
Figure. 8 An overview of supercapacitor types	25
Figure. 9 A model of an electrical double layer forming at a negatively charged surface	26
Figure. 10 Reversible redox reactions occurring on a pseudocapacitor surface.....	27
Figure. 11 The relationship between relative humidity (A) and light power transmission (B) in the sensor over time	28
Figure. 12 A schematic for the exfoliation process of MoS ₂	30
Figure. 13 DLS results for various IPA concentrations in water for MoS ₂ exfoliation. A) used a IPA:Water ratio of 2:8 B) a ratio of 3:7 C) a ratio of 4:6	36
Figure. 14 DLS results for various sonication times for MoS ₂ exfoliation. A) used a sonication time of 3x2 hrs B) used 3x3 hrs	37
Figure. 15 DLS results for varying sonication amplitudes A) is bath sonication B) tip sonication at 20% C) tip sonication at 30%	38
Figure. 16 AFM images of exfoliated MoS ₂ A) MoS ₂ exfoliated by bath sonication B) 20% amp tip sonication C) 30% amp tip sonication	39
Figure. 17 TEM images of exfoliated MoS ₂ A&B) bath sonication C&D) 20% tip sonication E&F) 30% tip sonication	40
Figure. 18 TEM SAED image of MoS ₂ produced by 30% amplitude tip sonication	40
Figure. 19 A) AFM of Intercalated and exfoliated MoS ₂ B) Height profile of the AFM image	42
Figure. 20 Raman spectra of bulk and exfoliated MoS ₂	43
Figure. 21 A-D SEM images of exfoliated MoS ₂	45
Figure. 22 (A & B) SEM back-scattering electron images with red arrows indicating deposits of MoS ₂ . (C) SEM image of the structure of the rGO/MoS ₂ aerogel composite. (D&E) SEM image of a pocket of MoS ₂ with elemental mapping.....	45
Figure. 23 CV plot between -0.8 and 0 V at 5mV s ⁻¹	46
Figure. 24 Galvanostatic charge-discharge plots of A) rGO aerogel and B) rGO/ MoS ₂ aerogel.....	47
Figure. 25 A) shows the capacitance and coulombic efficiency from 1 to 5000 cycles at 2 A g ⁻¹ B) The Nyquist plot for rGO/MoS ₂ electrode between 0.001 and 1000000 Hz.....	48
Figure. 26 AFM image of the MoS ₂	49
Figure. 27 SEM image of the sensor surface	50

Figure. 28 Change is resistance vs time of both MoS₂ film and the composite. 50

Figure. 29 Electrical resistance vs time with nitrogen exposure 51

Tables

Table. 1 Structural data for MoS ₂ phases	16
Table. 2 A table showing the average particle size for all IPA concentrations	36
Table. 3 A table showing the average particle size for all sonication times	37
Table. 4 A table showing the average particle size for all sonication amplitudes	38
Table. 5 Comparison of exfoliation methods in the literature and this work.....	41
Table. 5 Table of the calculated values of capacitance (C) and coulombic efficiency (ϵ)	47

List of abbreviations

TMD – Transition metal dichalcogenide
rGO – Reduced graphene oxide
GO – Graphene oxide
PMMA – Poly(methyl methacrylate)
MFC – Microfiber cellulose
LPE – Liquid phase exfoliation
CVD – Chemical vapour deposition
IPA – Isopropanol/propan-2-ol
NMP – N-methyl-2-pyrrolidone
DMF – Dimethylformamide
DMSO – Dimethyl sulphoxide
THF – Tetrahydrofuran
n-BuLi – n-butyllithium
t-BuLi – Tert-Butyllithium
MeLi – Methyllithium
LiOH – Lithium hydroxide
EtOH - Ethanol
SEM – Scanning electron microscopy
TEM – Transmission electron microscopy
AFM – Atomic force microscopy
DLS – Dynamic light scattering
EDL – Electrical double layer
CV – Cyclic voltammetry
EIS – Electrochemical impedance spectroscopy
G – Gibb's free energy
H – Enthalpy
T – Temperature
S – Entropy
V – Volume
IR – Infrared

δ – Nanosheet thickness
 Φ – Volume fraction
 D – Translational diffusion coefficient
 k – Boltzmann's constant
 F – Force
 k_c – spring constant
 δ_c – Cantilever deflection
 Z – Distance
 Γ – Phonon mode
 Ψ – electrical potential
 C – Capacitance
 ϵ_r – Dielectric constant
 ϵ_0 – Permittivity of a vacuum
 d – Debye length
 A – Surface area
 F – Farads
 V – Volts
 A – Ampere
 W – Watts
 Hz - Frequency
 s - Secounds
 h – Hours
 min – Minutes
 ppm – Parts per million
 rpm – revolutions per minute
 amp – Amplitude

1.1 Resumo:

A preparação química do MoS₂ 2D a partir do mineral foi investigada neste trabalho com o objetivo de disponibilizar um nanomaterial para dispositivos de energia e sensoriamento. Um método para esfoliação do MoS₂ foi desenvolvido testando-se o efeito da variação de parâmetros da sonicação em um solvente misto de IPA e água. Uma proporção de 3:7 IPA e água e uma intensidade de sonicação específica de 30% de 130 W e 20 KHz foi a parametrização que forneceu os resultados mais favoráveis quando obtidas uma ou muito poucas camadas de MoS₂ com um tamanho lateral razoável de 400 a 500 nm. Estas nanofolhas foram caracterizadas utilizando-se espalhamento dinâmico de luz em suspensão e o material depositado foi caracterizado por microscopia de força atômica, microscopia eletrônica de transmissão, microscopia eletrônica de varredura e espectroscopia Raman.

Através da modificação da esfoliação do MoS₂ pela intercalação de íons de Li⁺ em nanofolhas de MoS₂, um novo eletrodo para supercapacitor foi estudado. Um composto de óxido de grafeno reduzido (rGO) e MoS₂ foi preparado, este composto envolveu a síntese de um aerogel por uma auto-organização redutiva de GO; MoS₂ foi depositado sobre este aerogel e suas propriedades eletroquímicas foram sondadas. Um aerogel de rGO puro e um de rGO/MoS₂ foram ambos estudados para comparar seu desempenho como eletrodos para um supercapacitor. Os dispositivos supercapacitores de aerogel utilizando eletrólito de Li₂SO₄ foram caracterizados utilizando voltametria cíclica, carga-descarga galvanostática e espectroscopia de impedância eletroquímica. O supercapacitor baseado em eletrodos compósitos de aerogel rGO/ MoS₂ forneceu uma capacitância de 140.4 F g⁻¹, que foi um aumento de 62% em relação ao eletrodo de aerogel de rGO puro e uma retenção de capacitância de 85% após de 5000 ciclos.

Um sensor de umidade foi desenvolvido utilizando MoS₂ esfoliado e microfibras de celulose. Este sensor foi muito sensível ao vapor de água no ar e respondeu rapidamente à presença de umidade, tornando-se muito mais condutor, com a resistência do dispositivo caindo em torno de 25%. O sensor retornava à sua resistividade de repouso de cerca de 100 MΩ quando exposto ao N₂.

Palavras-chave: MoS₂, esfoliação em fase líquida, rGO, supercapacitor, sensor de umidade, compósitos, microfibras de celulose

1.2 Abstract:

The chemical preparation of the 2D MoS₂ from the mineral was pursued in this work with the aim of making available a nanomaterial for energy and sensing devices. A method for exfoliation of MoS₂ was developed by testing the effect of differing parameters of sonication in a mixed solvent of IPA and water. A ratio of 3:7 IPA and water and a specific sonication intensity of 30% of 130 W and 20 KHz was found to give the most favourable results where mono and very few layer MoS₂ with a reasonable lateral size of 400 to 500 nm were obtained. These nanosheets were characterised using dynamic light scattering in suspension and the deposited material was characterised by atomic force microscopy, transmission electron microscopy, scanning electron microscopy and Raman spectroscopy.

Through the modification of the exfoliation of MoS₂ by intercalation of Li⁺ ions to the MoS₂ nanosheets, a novel electrode for supercapacitor was studied. A composite of reduced graphene oxide (rGO) and MoS₂ was prepared, this composite involved synthesising an aerogel by a self-assembly reduction of GO, MoS₂ was deposited onto this aerogel and its electrochemical properties were probed. An aerogel of pure rGO and an rGO/MoS₂ were both studied to compare their performance as electrodes for a supercapacitor. The aerogel supercapacitor devices using Li₂SO₄ electrolyte were characterised using cyclic voltammetry, galvanostatic charge-discharge and electrochemical impedance spectroscopy.

The supercapacitor based on rGO/MoS₂ aerogel composite electrodes gave a capacitance of 140.4 F g⁻¹ which was an increase of 62% over the pure rGO aerogel electrode and a capacitance retention of 85% after 5000 cycles.

A humidity sensor was developed by using exfoliated MoS₂ and microfiber cellulose. This sensor was very sensitive to water vapour in the air and would respond very quickly to the presence of humidity by becoming much more conductive with the resistance of the device dropping by around 25%. The sensor would return to its resting resistivity of around 100 MΩ when exposed to N₂.

Keywords: MoS₂, liquid phase exfoliation, rGO, supercapacitor, humidity sensor, composites, microfiber cellulose

2. Introduction

The development of nanomaterials since the beginning of the 21st has stimulated major growth of research and industrial interest in nanotechnological solutions to problems currently facing civilisation. The discovery of graphene in 2004¹ opened a new frontier in science. Two-dimensional materials have become the focus of a wide range of subjects and have also promoted the search for more materials like graphene. One such class of materials are the transition metal dichalcogenides (TMD), these compounds have the general formula MX_2 where M is typically a group 5 or 6 transition metal (Mo, W, V etc.) and X is a chalcogen (S, Se or Te).² The TMDs, like graphene, are layered materials consisting of sheets of metal atoms sandwiched by chalcogen atoms stacked upon each other, these sheets are held together by weak van der Waals forces. The bulk material is relatively uninteresting only seeing research in applications such as lubricants, the group 6 TMDs only seeing collectively less than 100 scientific article publications per year before 2010. However, with advancements in preparation and understanding of the enhanced and emergent properties of monolayer TMDs, this has increased substantially to over 300 publications per year as of 2019 in areas ranging from energy storage, sensors and catalysis.³

As the population of the earth is steadily increasing and more nations become industrialised, the energy demand is constantly rising. In 2016, 80% of energy production remains as non-renewable fossil fuels.⁴ A big obstacle preventing the transition to fully green renewable energy is the current problem of energy storage and conversion technology. Nanomaterials have the potential to influence humanity's future in this regard. The TMDs potentially offer solutions to these problems and research into the TMD molybdenum disulphide (MoS_2) has made excellent progress in energy storage, examples of this are studied by Chang et. al.⁵ for example, The group studied that a MoS_2 /graphene composite as a lithium-ion battery gave a specific capacity of $\sim 1100 \text{ mAh g}^{-1}$ and in another example, Pazhamalai et. al.⁶ studied a few layer MoS_2 symmetric supercapacitor with a specific capacitance of 14.75 F g^{-1} and an energy density of 18.43 Wh kg^{-1} . These studies highlight how a material such as MoS_2 will potentially usurp current technologies or at the very least will lead to the development of a class of materials that will.

In this dissertation, a literature review outlines the properties, preparation and applications of MoS₂. The objectives of the work are outlined in chapter 4, Chapter 5 details the methodology used throughout the work and Chapter 6 discusses the results of MoS₂ exfoliation, supercapacitor device and gas sensor. Finally, the last two chapters include the conclusions and bibliographical references.

3. Literature Review

3.1 Two-dimensional MoS₂:

Two-dimensional materials have seen an enormous spike in interest since the beginning of the 21st century, stimulated by the first production of single-atom-thick graphene in 2004 by Novoselov et al.¹ Graphene gained interest due to its extraordinary properties⁷ and its potential in future applications in a wide variety of fields. However, graphene is not the only material of significance. Transition metal dichalcogenides (TMDs) consisting of metal atoms (M) sandwiched between two layers of chalcogen atoms (X) MX₂, where M is typically Mo, W, Nb, Re, Ni or V and X is typically S, Se or Te.⁸ Molybdenum disulphide (MoS₂) is one such TMD that has seen much research in the last 10 years (especially with in the last 4-5 years).

Nanomaterials are typically considered to be a material where a single unit of said material falls into the 1-100 nm range of size. This is significant because at this scale quantum fluctuations that are normally averaged out in larger materials will become more apparent, especially when considering materials with lower dimensions (2D materials).⁹ Moreover, the high surface area of nanomaterials is an important factor in applications. For example, there are many active sites for sensing and catalysis also many sites for ion intercalation or electrochemical interactions for energy storage¹⁰ graphene has been found to have a specific surface area of 2630 m² g⁻¹ which is recognised as being exceptionally high¹¹ and MoS₂ having a 636 m² g⁻¹ theoretical specific surface area.¹²

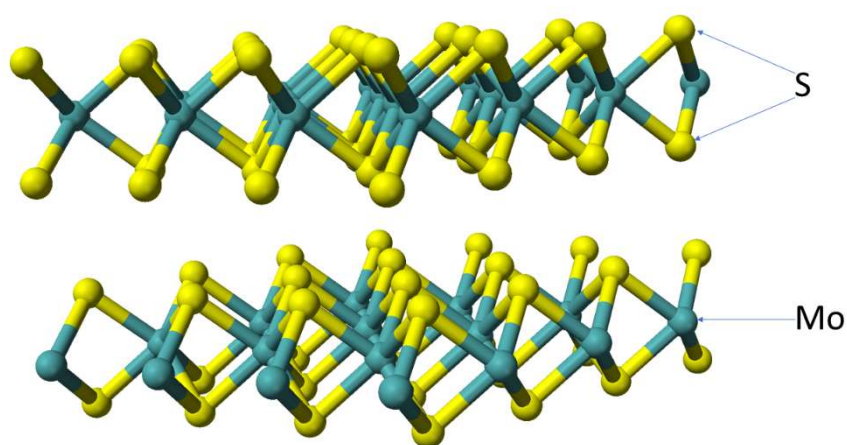


Fig.1. 3D ball and stick model of 2H-MoS₂.

MoS₂ has several crystalline phases, the bulk material exists in two phases 2H-MoS₂ and 3R-MoS₂, where H and R indicate hexagonal and rhombohedral symmetry. This bulk material consists of many layers of MoS₂ stacked and held together by weak van der Waals forces. Both 2H- and 3R-MoS₂ has a structure of a uniform plane of Mo atoms sandwiched above and below by S atoms, each Mo atom has 6 S atoms coordinated in a trigonal prismatic geometry as shown in Fig. 1. The third phase 1T-MoS₂ can only exist in the monolayer form and is in the octahedral geometry 1T-MoS₂ and can only be produced by inducing the phase change by intercalation of alkali metals, commonly Li.¹³ Table. 1. Shows the structural data for the phases of MoS₂, the lattice parameters of 1T-MoS₂ varies depending on the method of preparation.¹⁵

MoS ₂ phase	Geometry	Lattice parameters (nm)
2H	Trigonal prismatic (D _{3h})	a = 0.316 c = 1.23 ¹⁴
3R	Trigonal prismatic (D _{3h})	a = 0.316 c = 1.84 ¹⁴
1T	Octahedral (D _{3d})	a = 0.316, 0.327, 3.36 c = 0.615, 0.629 ¹⁵

Table. 1. Structural data for MoS₂ phases

Both 2H and 3R-MoS₂ are semiconductors with an indirect band gap of 1.24 eV¹⁶ However, when exfoliated and as a monolayer crystal, MoS₂ will have a direct bang gap of 1.9 eV.¹⁷ 1T phase is highly conductive, up to 10⁷ times more than 2H-MoS₂.¹⁸ 1T-MoS₂ is metastable and will convert back to 2H-MoS₂ after 2 months of aging or annealing at temperatures of 300°C after as little as 1 h.¹⁹ Methods for stabilising the 1T phase have been reported with WS₂ and theoretically with MoS₂ nanotubes.²⁰

The electronic properties of MoS₂ can be explained by applying ligand field theory²¹, 2H and 3R MoS₂ are semiconducting due to the filled d_{z²} orbital and the empty d_{xy} and d_{x²-y²} orbitals as seen in Fig. 2. A which gives rise to its band gap. However, the 1T-MoS₂ is more conductive because of its partially filled t_{2g} band as seen In Fig. 2. B this gives the MoS₂ in this phase a metallic characteristic.

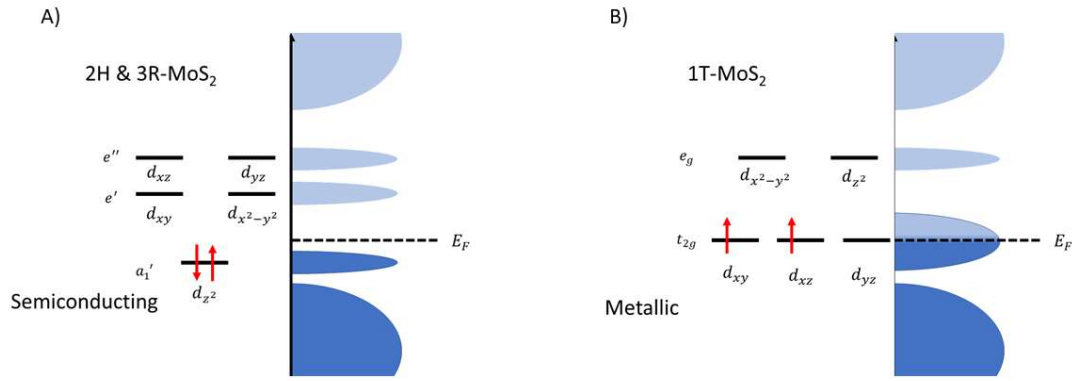


Fig.2 A) Ligand field splitting for trigonal prismatic MoS₂ and B) octahedral MoS₂

There are a few ways in which MoS₂ can be exfoliated from bulk material to produce the few-monolayered MoS₂. Liquid-phase exfoliation (LPE) is a common method²² which involves suspending the material in a suitable solvent and separating the layers with mechanical work such as sonication²³ and shear.²⁴ Chemical vapour deposition (CVD) involves synthesising the MoS₂ (usually from MoO₃) and depositing the product onto a surface as thinly as possible.²⁵ While both methods are valid they usually see differing applications.

3.2 Preparation of MoS₂:

Backes et al. outlined a guideline for exfoliation²⁶ LPE allows for the production of around 1 to 10 layers and ideally around 100 nm – 100 μm. To perform LPE it is necessary to first identify a suitable solvent.²⁷ It is important to consider the surface energy of the material, for this the relationship between solvent and solute can be understood via the eqn (1):²⁸

$$\Delta G_{mix} = \Delta H_{mix} - T\Delta S_{mix} \quad (1)$$

Where: ΔG_{mix} is the free energy of mixing. ΔH_{mix} is the enthalpy of mixing, Finally ΔS_{mix} is the entropy of mixing. Therefore, if ΔG_{mix} is negative then the mixing of the material with the solvent is favourable. Because the exfoliated material is two-dimensional, the interaction between the solvent and nanosheets will be primary on the basal plane.²² The balance of the van der Waals interaction in this system can be explained by the eqn (2):²⁹

$$\frac{\Delta H_{mix}}{V} = \frac{2}{T_{NS}} (\delta_s - \delta_{NS})^2 \Phi \quad (2)$$

Where: T_{NS} is the nanosheet thickness δ_s and δ_{NS} are the surface energy of the solvent and the nanosheets and Φ is the volume fraction of the dispersed nanosheets.

It is very common to exfoliate MoS₂ via the sonication method, this involves dispersing MoS₂ in the suitable solvent then treating with a tip or bath sonicator. This process works by the tip or bath sonicator creating small cavitation bubbles that will collapse and send shockwaves and microjets through the solvent, these shockwaves will encounter the MoS₂ particles and break the weak van der Waals forces between the layers and exfoliate the MoS₂ to produce nanosheets. The sonication process will also fragment the particles and produce nanosheets with differing diameters.³⁰

When exfoliating MoS₂ solvents such as N-methyl-2-pyrrolidone (NMP) and dimethylformamide (DMF) are widely used throughout the literature due to the factors mentioned above and because they are high-boiling point solvents, which is particularly useful when exfoliating via the use of sonication.³¹⁻³⁴ However, there is worldwide concerns over the use of solvents such as NMP due to its toxicity. Much work in recent years has attempted to find an ideal way to exfoliate MoS₂ using less toxic and less environmentally harmful solvents, such as using alcohols and/or water.³⁵⁻³⁷



Fig. 3. An overview of the exfoliation route of MoS₂

Smith et al.³⁸ exfoliated MoS₂ in water using a tip sonicator with the use of the surfactant sodium cholate as a stabiliser. The dispersions were sonicated for 30 min then centrifuged for 90 min at 1500 rpm. This allowed the group to obtain exfoliated MoS₂ with average lateral sizes of 280 nm with 2 to 9 layers. Ma et al.³⁹ were able to exfoliate MoS₂ in pure water without the use of a stabiliser. This involved sonication at high power (130 W) for an extended period of 8 h followed by centrifugation at 1500-3000 rpm. The group demonstrated that in this process MoS₂ nanosheets with sizes between 100-400 nm could be obtained. Although, these nanosheets were found to be a mixture of few-layer MoS₂ with 5-6 layers and many-

layer MoS₂ with 15-20 layers. Fast sedimentation was reported at low centrifugation speeds was reported with a significant decrease in colloid concentration in two weeks. However, stable suspensions were reported at high centrifuge speeds. It was also reported that sonication would break Mo-S bonds due to fragmentation, this allows the edges to react with water and form hydrophilic groups improving the interaction between the nanosheets and the water molecules.

Zhou et al.⁴⁰ conducted a theoretical study by simulating MoS₂ exfoliation in a mixture of water and IPA (1:1 ratio). The simulation suggests that collapsing cavitation bubbles send high energy jets through the solvent and when they impact MoS₂ it will increase the surface temperature to around 3000 K and the pressure to 20 GPa which gives a shear stress of 10 GPa. This will initiate the exfoliation process.

Backes et al.⁴¹ demonstrated an exfoliation in pure IPA, with a sonication time of 5 h and centrifugation to isolate exfoliated and unexfoliated material. The group were able to produce nanosheets with average lateral sizes of 260 nm and 9-10 layers. This study shows at the least that exfoliation using IPA is indeed possible.

While, directly sonicating bulk MoS₂ is common, very often studies will first intercalate MoS₂ with Li⁺ ions. This is specially used when the aim is to study the application of exfoliated MoS₂ in energy storage devices.

Intercalation and removal of Li⁺ in MoS₂ induces the phase transition between 2H-MoS₂ and 1T-MoS₂. This transition is outlined in Fig. 4, upon insertion of Li ions the H-MoS₂ will remain stable and be the dominant phase, however, once the Li concentration in the MoS₂ active sites reaches 20% the octahedral MoS₂ will become more stable and the phase transition will initiate (given the symbol in this figure O-MoS₂). Once all active sites are occupied by Li ions the dominate phase will be the metallic octahedral MoS₂ (given the symbol DT-MoS₂). With the removal of the Li ions, the octahedral MoS₂ (ZT-MoS₂) will remain octahedral for some time, however, upon heating and/or aging will revert to H-MoS₂.⁴²

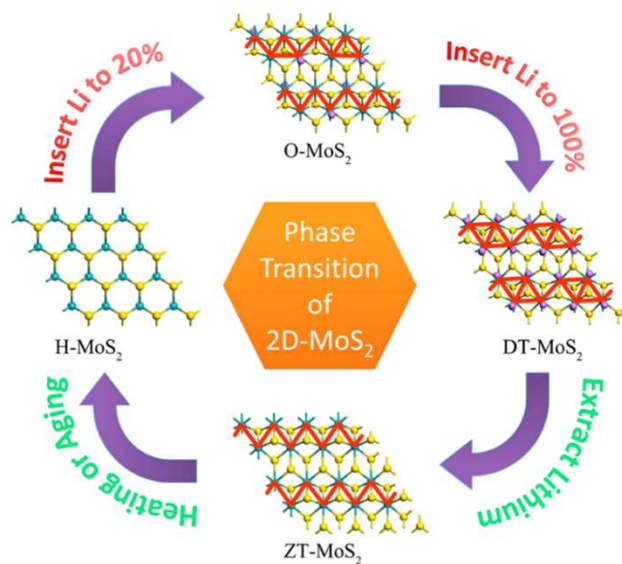
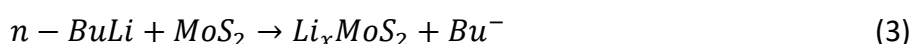


Fig. 4. Pathway of phase transitions for MoS₂.⁴²

Two common ways of interaction of MoS₂ with Li⁺ are chemical and electrochemical routes.

The chemical route of Li⁺ intercalation can be achieved by mixing bulk MoS₂ with an organolithium compound. n-butyllithium (n-BuLi) and tert-butyllithium (t-BuLi) have been shown to be much more effective for intercalation of MoS₂ than smaller organolithiums such as methyl lithium (MeLi).⁴³ A typical intercalation using n-BuLi will involve adding MoS₂ powder to a solution of n-BuLi (usually around 1.5 M) in hexane and storing for several days in an inert atmosphere.⁴⁴ The reaction is showed in eqn (3):



The alternative route is the electrochemical method. This method involves using MoS₂ as a working electrode in a lithium electrolyte and passing a constant current between the working and counter electrode, in a galvanostatic discharge mode.⁴⁵ In this process the Li⁺ will move into the gap between the sheets. The Li⁺ is reduced and Li_xMoS₂ is formed. This method has an advantage as the fine tuning of the degree of intercalation can be controlled by using the galvanostatic curves as shown in Fig. 5. The voltage here decreases from 1.8 to 1.2 V until x=0.2 here it will plateau indicating the phase transition.

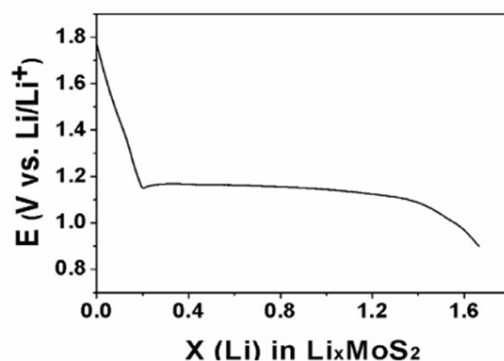


Fig. 5. Galvanostatic discharge curve for Li intercalation of MoS_2 ⁴⁵

3.3 Characterization of MoS_2 :

Characterisation of exfoliated MoS_2 is a very important step before considering applications, for example, scanning electron microscopy (SEM) and atomic force microscopy (AFM) are essential for determining the lateral sizes of exfoliated nanosheets and the thickness (and therefore number of layers in the nanosheet). AFM is particularly useful for this.

Dynamic light scattering (DLS) is often the first technique used, this is because it is a characterisation that is conducted on the colloidal suspension itself. DLS allows probing of the Brownian motion in colloidal suspensions. As the particles move throughout the solvent the instrument will measure the spatial light scattering intensity distribution as a function of time, this intensity will be constantly fluctuating due to the movement of the particles.⁴⁶ By applying the auto-correction of this intensity, distribution information about the motion of the particles in the suspension and the translational diffusion coefficient can be calculated.⁴⁷ The diameter of the particles can therefore be calculated by solving for the hydrodynamic radius using the Stokes-Einstein eqn 4:

$$D = \frac{kT}{6\pi\eta a} \quad (4)$$

Where D is the translational diffusion coefficient, k is the Boltzmann constant, T is temperature, η is the viscosity of the liquid and a is the hydrodynamic radius. The hydrodynamic radius is diameter of the particles redefined as hard spheres diffusing through the medium at the same rate. While particles like MoS_2 are not spherical using the hydrodynamic radius is a sufficient approximation for determining the average particle diameter.⁴⁸

AFM is a very common method used in studies of nanomaterials. AFM is very useful for materials on this scale as it can attain a resolution in picometer scale⁴⁹, this allows very accurate measurements of the materials thickness. AFM works by running a cantilever with a very sharp probe across a surface of interest, this probe which is typically made of silicon has a radius on the order of nanometres. As this tip is moved along the surface of the sample, the deflection of the cantilever caused by the forces between the tip and the sample is described by Hooke's law⁵⁰ in eqn (5):

$$F = -k_c \delta_c \quad (5)$$

Where F is the force, k_c is the spring constant of the cantilever and δ_c is the cantilever deflection. The actual tip-sample distance cannot be calculated this way as this does not give the actual distance between the tip and the sample. Applying the correction in eqn (6):

$$D = Z - (\delta_c + \delta_s) \quad (6)$$

Where Z is the distance between the sample and the surface that the sample is deposited on and δ_s is the cantilever deflection on the sample, this is shown in Fig. 6.

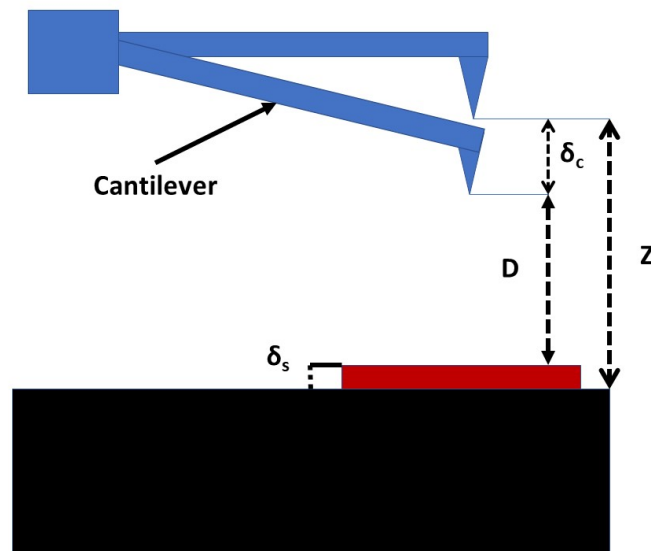


Fig. 6. AFM cantilever and sample system

For measuring the thickness of nanomaterials and therefore determining the number of layers it is necessary to use tapping mode AFM. This method is highly utilised to determine the number of layers of exfoliated MoS₂.⁵¹⁻⁵³

SEM is also a method used to evaluate lateral size as well as morphological features, however, by evaluating other signals produced by SEM for example, secondary electrons and backscattering electrons information about the nanosheets can be obtained.

TEM is widely used to characterise MoS₂ nanosheets as it gives a very high-resolution information about aspects such as shape lateral size and morphology, especially compared to SEM. TEM works by transmitting a beam of electrons through a thin sample of in this case a MoS₂. Depending on the thickness of the sample the electron transparency will vary.⁵⁴

A very important aspect of using TEM is performing selected area electron diffraction (SAED). This technique is important as it allows the determination of the crystal structure of the nanomaterial. This is significant in studying MoS₂ as it allows observation of the difference in crystal structure between 2H-MoS₂ and 1T-MoS₂.⁵⁵ By evaluating the electron diffraction patterns as the interaction of MoS₂ with Li results in the distortion of MoS₂ basal planes. In bulk MoS₂ the (001) planes are parallel with a separation of 0.615 nm, with Li intercalation this spacing becomes wider.

One important characterisation technique is Raman that is used to study structural and electronic properties of MoS₂ by light scattering by phonons. Bulk MoS₂ and monolayer MoS₂ differ in that their primitive cells contain 6 and 3 atoms respectively which gives 18 phonon modes for bulk MoS₂ and 9 for monolayer MoS₂ shown in eqn (7&8):⁵⁶

$$\Gamma_{optical}(bulk MoS_2) = A_{2u}(IR) + E_{1u}(IR) + A_{1g}(R) + 2E_{2g}(R) + E_{1g}(R) + 2B_{2g}(IN) + B_{1u}(IN) + E_{2u}(IN) \quad (7)$$

$$\Gamma_{optical}(monolayer) = A'_2(IR) + E'(IR + R) + A'_2(R) + E''(R) \quad (8)$$

Where (IR) are infrared modes, (R) are Raman modes and (IN) are inactive or silent modes. The two main peaks for MoS₂ are the A_{1g} and E_{2g}¹ which correspond to out-plane and in-plane vibrational modes, respectively. The distance between the two main peaks can be used to estimate the number of layers of the nanosheets. Once the material is exfoliated down to

four or less layers, these two peaks become sensitive to change and will move closer to each other, the degree to which will depend on the number of layers.⁵⁷

3.4 Applications for 2D MoS₂:

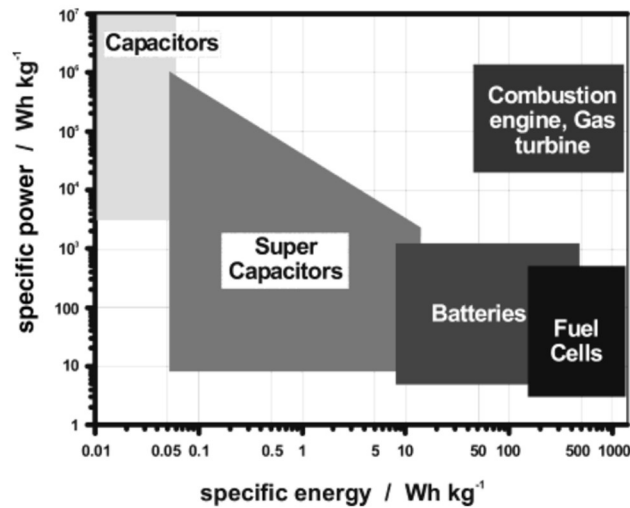


Fig. 7. Ragone plot of energy storage devices.⁵⁸

For MoS₂ and other TMDs an application that has gained enormous interest is energy storage, this area of research is very important as an increasing concern worldwide for the environment has caused unprecedented shifts in the global attitude to energy policies.⁵⁹ It has become very important to consider renewable energy sources e.g. solar and wind. These energy sources show a lot of promise; however, these sources depend heavily on weather conditions and time of day, therefore, energy storage devices are a key focus of research. One such energy storage device that has attracted a lot of interest are supercapacitors. Supercapacitors are devices that bridge the gap of energy density and power density of batteries and electrostatic capacitors^{60,61} as illustrated in Fig. 7.

5.4.1 Supercapacitors:

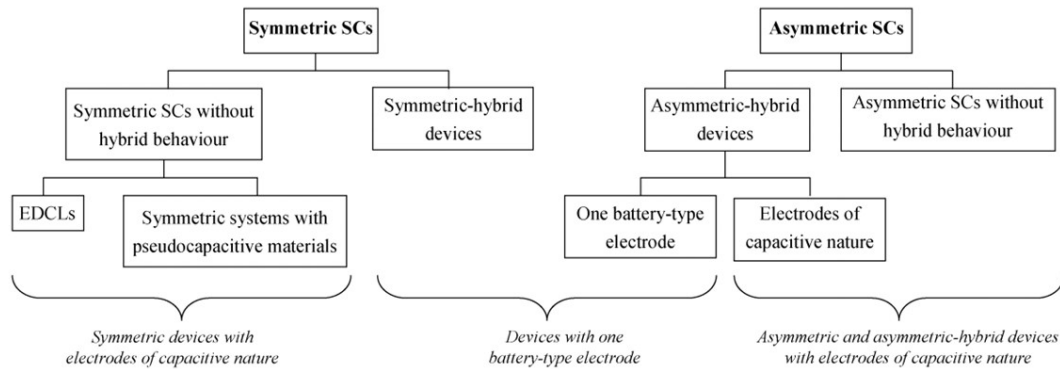


Fig. 8. An overview of supercapacitor types⁶²

Supercapacitors come in three main types as shown in Fig. 8. Electrochemical double-layer capacitors (EDLCs), pseudocapacitors and hybrids.

Double-layer capacitor:

EDLCs store charge primarily by forming electric double-layers first described by Helmholtz in 1853⁶³ where an interface of two layers of charge form on the surface of a colloid system.

The behaviour of the ions in an electrical double layer as shown in fig. 9. can be described with the following equation:

$$\varphi(x) = \varphi_s e^{-kx} \quad (9)$$

Where $\Psi(x)$ is the distribution of the electrical potential, Ψ_s is the surface potential and k is the Boltzmann's constant. An EDCL supercapacitor will hold charge by maintaining this double layer with the surface potential, when this surface potential is lost the electrical double layer will dissociate, and the supercapacitor will discharge.

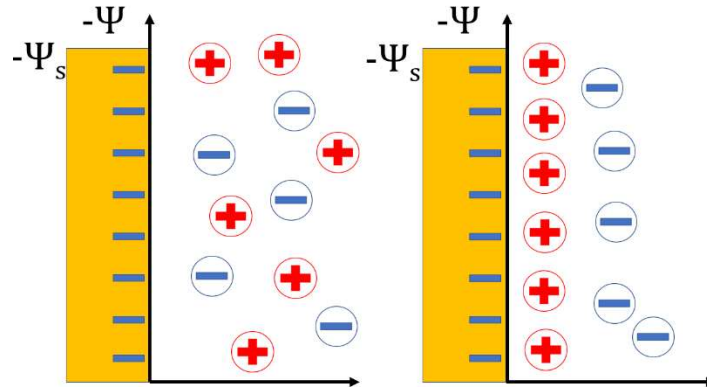


Fig. 9. A model of an electrical double layer forming at a negatively charged surface

The capacitance of an EDLC supercapacitor can be estimated using the following equation⁶⁴:

$$C = \frac{\epsilon_r \epsilon_0}{d} A$$

Where, ϵ_r is the dielectric constant of the electrolyte, ϵ_0 is the permittivity of a vacuum, d is the Debye length and A is the specific surface area. The equation shows that capacitance will increase linearly with increasing specific surface area, for this reason highly porous carbon materials have been identified as great materials for this application.⁶⁵⁻⁶⁸

Pseudocapacitors:

Pseudocapacitors differs from EDLCs as the charge storage mechanism is based on fast reversible redox reactions. This offers some advantages, for example the capacitance can be higher than an EDLC. However, the supercapacitor will have low power density as the materials will have a lower conductivity and they will be less stable during cycling due to damage to the electrodes surface.⁶⁹

Metal oxides such as ruthenium oxide (RuO_2),⁷⁰ manganese dioxide (MnO_2)⁷¹ and vanadium pentoxide (V_2O_5)⁷² have been studied as pseudocapacitor electrode materials. These metal oxides exhibit good pseudocapacitance behaviour as reversible redox reactions can occur on their surfaces shown in Fig. 10.

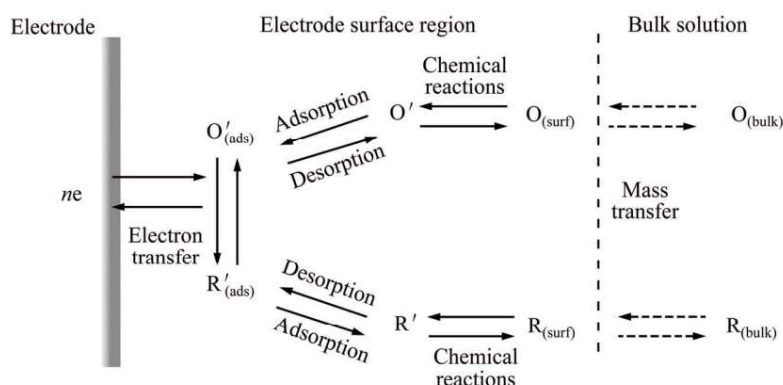


Fig. 10. Reversible redox reactions occurring on a pseudocapacitor surface.⁷³

MoS₂ as a supercapacitor material:

MoS₂ can be integrated into a supercapacitor. MoS₂ is of interest due to its high surface area and its analogous structure to graphene. Furthermore, MoS₂ has a higher ionic conductivity⁷⁴ and a higher theoretical capacitance.⁷⁵ MoS₂ is often used as a composite as an electrode material, common components of the composites are graphene⁷⁶⁻⁷⁸ and its derivatives, especially reduced graphene oxide (rGO).⁷⁹⁻⁸¹ Some composites have also incorporated transition metals.⁸² Xu et al.⁸³ developed a supercapacitor electrode material that is made up of NiS, rGO and MoS₂ and was able to achieve a capacitance of 2225 F g⁻¹ at 1 A g⁻¹ and 1347.3 F g⁻¹ at 10 A g⁻¹ while maintaining 94.5% of initial capacitance after 50,000 cycles.

The structure of MoS₂ makes it very flexible, meaning that there is much interest into investigating wearable technology. Cocuzza et al.⁸⁴ Investigated a wearable supercapacitor made of an rGO aerogel and MoS₂ 10.3 mF cm⁻¹ at 100 mV s⁻¹ was achieved.

5.4.2 Humidity sensors:

Nanomaterials like MoS₂ have seen much interest in sensor devices in recent years.⁸⁵ Humidity sensors are of particular interest as high humidity especially in an indoor closed environment can adversely affect health.⁸⁶ There are two main types of humidity sensor: impedance type sensors and capacitive type sensors.

Impedance sensors are typically based upon interdigital electrodes,⁸⁷ where a material is deposited between two electrodes. These sensors will measure change in humidity by measuring a change of electrical impedance of the sensing material. When water molecules are absorbed onto the surface of the sensor, the molecules are dissociated into the ionic hydroxyl groups and the conductance of the material is increased.⁸⁸ The capacitive sensors can be constructed similarly to impedance type sensors interdigitally, these sensors work by responding to varying humidity by the change of the materials dielectric permittivity.⁸⁸

MoS₂ is a promising candidate for gas sensing devices, Kim et al.⁸⁹ developed a very sensitive O₂ sensor using MoS₂ nanoparticles, the sensor would respond by becoming much more resistant when high concentrations of O₂, the sensor would return to its resting resistance very fast when exposed to N₂. Lee et al.⁹⁰ developed a NH₃ sensing device that could respond to NH₃ at concentrations as low as 2 ppm.

MoS₂ is a viable gas sensing material due to its high surface area and most notably for water sensing the edge sites that will react with water by means of hydrogen evolution.⁹¹ Li et al.⁹¹ noted that pure MoS₂ does not show a satisfactory humidity sensing property, this group used an MoS₂/Ag composite film, this film was very sensitive to water and had a very quick response time (~1.5 s). Du et al.⁹² demonstrated how a humidity sensor made of MoS₂ could be used to monitor human breath by through measuring relative humidity, the transmission of light power will vary depending on the relative humidity as shown in Fig. 11.

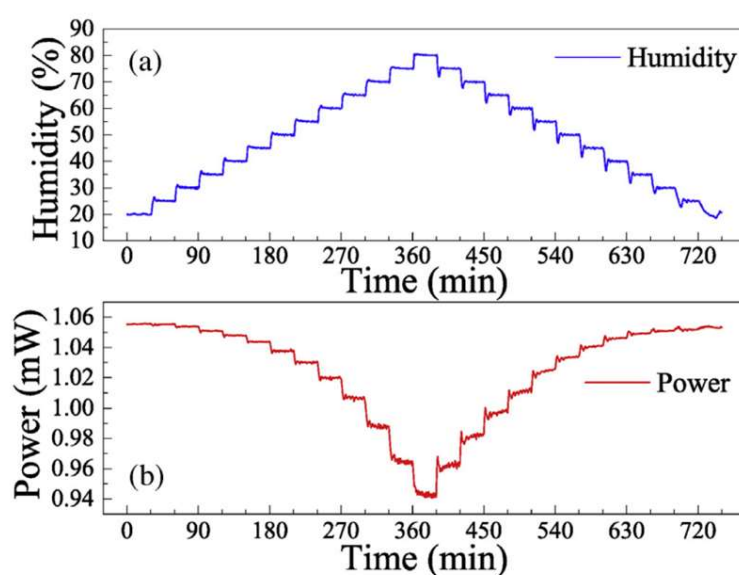


Fig. 11. The relationship between relative humidity (A) and light power transmission (B) in the sensor over time.⁹²

4. Objective

General objectives:

The general objective of this project was to find a less harmful way to prepare exfoliated MoS₂ dispersed in a medium and apply the nanomaterial in devices such as for energy storage and sensing.

The goal was to exfoliate MoS₂ down to few-monolayer nanosheets and to investigate the parameters that will lead to a fine tuning of nanosheet thickness and diameter. Once MoS₂ suspensions were produced, the applications of the MoS₂ nanosheets were investigated.

Specific objectives:

- Develop a greener method for suspending and exfoliating MoS₂ using sonication. Characterise the exfoliated MoS₂ to determine if the method has developed few-monolayer MoS₂. In this context, particle size was evaluated using differing parameters in the exfoliation process optimization: type of solvent, method of sonication, time and intensity of sonication treatment.
- Investigate potential applications in which this method can be integrated. Evaluate the potential for the material to be used as a supercapacitor electrode material with advantages in the device performance. Evaluate the potential for the nanomaterial to be used in a novel gas sensing device.

5. Methodologies

Production of exfoliated MoS₂ from bulk MoS₂:

Preliminary exfoliation experiments:

In this early work, exfoliation of MoS₂ (Sigma) was attempted in tetrahydrofuran (THF) mixed with Poly(methyl methacrylate) (PMMA) based on the work of May et Al.⁹³ 5 g of bulk MoS₂ and 50 g of PMMA was mixed in 10 mL of THF and was sonicated for 1 h at 130 W and 20 KHz. The suspension was centrifuged at 3500 rpm for 20 min and the supernatant was collected. This method was abandoned due to reasons discussed in the results and discussion.

Exfoliation with Isopropanol and water:

This section will outline the method used to exfoliate MoS₂ in a mixed solvent system of water and isopropanol (IPA). The overall exfoliation and characterization steps are showed in Fig. 12.

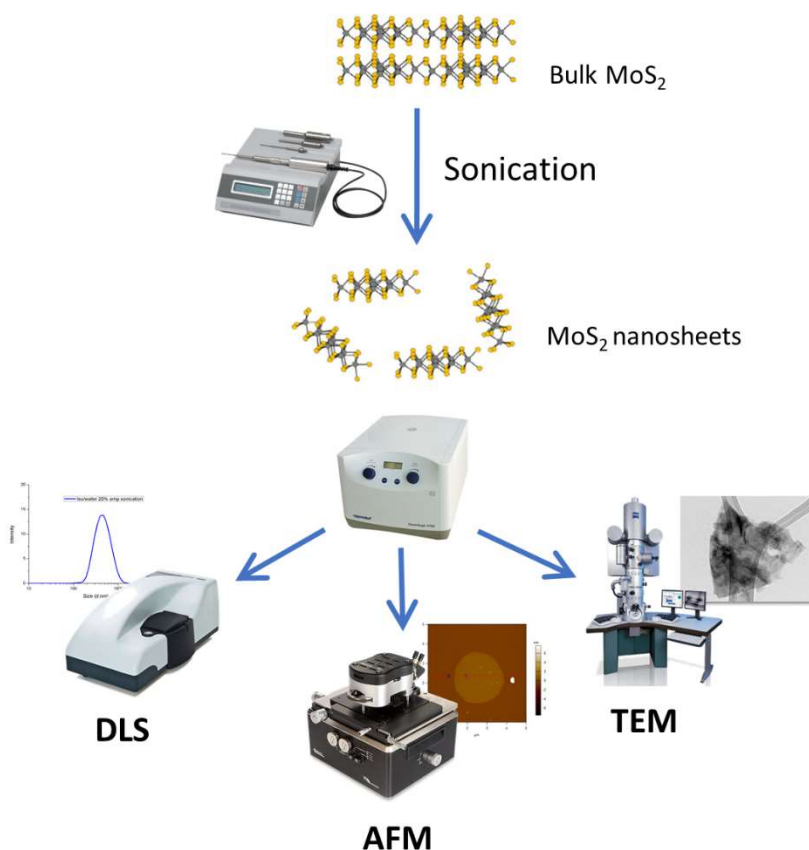


Fig. 12. A schematic for the exfoliation process of MoS₂.

Exfoliation of MoS₂ in differing ratios of Isopropanol and water:

In this work the effect on the ratio of water to IPA was investigated.

20 mL of IPA and 80 mL of water (2:8) was thoroughly mixed in a 250 mL beaker. 400 mg of MoS₂ was weighed and added to the mixed solvent. The mixture was subjected to tip sonication for 1 h (30% amplitude of 130 W and 20 KHz) and the resulting suspension was centrifuged at 2500 rpm for 20 min. The supernatant was collected and stored. The residue at the bottom of the falcon tube was collected and mixed again with 50 mL mixed solvent of 10 mL IPA and 40 mL of water and was sonicated for 1 h at the same amplitude and again the suspension was centrifuged at the same speed and for the same time. The supernatant of this sonication was collected and stored in the same bottle as the first exfoliation, the residue was collected and subjected to one more exfoliation using all the same parameters. 100 mL of the stored suspension was collected and centrifuged at 4000 rpm and decanted.

The same process was repeated with a mixed solvent of (3:7) and (4:6) ratio of IPA and water.

Exfoliation of MoS₂ in differing sonication times:

30 mL of IPA and 80 mL of water (3:7) was thoroughly mixed in a 250 mL beaker. 400 mg of MoS₂ was weighed and added to the mixed solvent. The mixture was subjected to tip sonication for 2 hrs (30% amplitude of 130 W and 20 KHz) and the resulting suspension was centrifuged at 2500 rpm for 20 min. The supernatant was collected and stored. The residue at the bottom of the falcon tube was collected and mixed again with 50 mL mixed solvent of 15 mL IPA and 35 mL of water and was sonicated for 2 h at the same amplitude and again the suspension was centrifuged at the same speed and for the same time. The supernatant of this sonication was collected and stored in the same bottle as the first exfoliation, the residue was collected and subjected to one more exfoliation using all the same parameters. 100 mL of the stored suspension was collected and centrifuged at 4000 rpm and decanted. The remaining 2500 rpm suspension and the 4000 rpm suspension was stored for characterisation.

The same process was repeated with a 3 h sonication time and 1 h sonication time however, in this process the sonication was only performed once.

Exfoliation of MoS₂ in differing sonication amplitudes:

30 mL of IPA and 80 mL of water (3:7) was thoroughly mixed in a 250 mL beaker. 400 mg of MoS₂ was weighed and added to the mixed solvent. The mixture was subjected to tip sonication for 1 h (20% amplitude of 130 W and 20 KHz) and the resulting suspension was centrifuged at 2500 rpm for 20 min. The supernatant was collected and stored. The residue at the bottom of the falcon tube was collected and mixed again with 50 mL mixed solvent of 15 mL IPA and 35 mL of water and was sonicated for 2 h at the same amplitude and again the suspension was centrifuged at the same speed and for the same time. The supernatant of this sonication was collected and stored in the same bottle as the first exfoliation, the residue was collected and subjected to one more exfoliation using all the same parameters. 100 mL of the stored suspension was collected and centrifuged at 4000 rpm and decanted.

This same process was also carried out in an ultrasonic bath using the same time of sonication and the same centrifuge parameters.

Characterisation:

Dynamic Light Scattering:

This technique was used to evaluate the material as a colloidal suspension. Dynamic light scattering (DLS) was used to determine the size and distribution of the MoS₂ in suspension. When the light strikes the particles of MoS₂ it will scatter via Rayleigh scattering, the Brownian motion causes the light to scatter at different intensities and introducing the Stokes-Einstein relation (eqn. 4) allows for the calculation of particle sizes. These experiments were carried out at the Laboratório de Encapsulamento Molecular e Biomateriais – LEMB (Laboratory of Molecular Encapsulation and Biomaterials) at the UFMG Department of Chemistry, using a Malvern instruments Zetasizer nano ZS Analyser.

Atomic Force Microscopy:

This technique was utilised to probe the morphological and height profile (and therefore number of stacked nanosheets) of deposited MoS₂. Atomic force microscopy (AFM) will sweep a silicon tip across a surface that has a deposited material. As the tip moves with topographical features the nanoscale movement of this tip is recorded. All samples were deposited onto a mica surface for characterisation the mode used for these measurements

was tapping. This was carried out at the Centro de Microscopia da UFMG (UFMG Microscopy Centre) using an Asylum Research MFP3D atomic force microscope.

Transmission Electron Microscopy:

This technique was used to gain detailed images of the MoS₂ nanosheets, and to further observe the layers of the MoS₂ nanosheets. Transmission electron microscopy (TEM) was performed at the Centro de Microscopia da UFMG (UFMG Microscopy Centre).

Intercalation and Exfoliation of bulk MoS₂:

Lithium Intercalation:

The electrochemical intercalation of MoS₂ was conducted by using a modified method used by Garah et al.⁹⁴

400 mg of bulk MoS₂ was pressed into a pellet 1.3 cm in diameter and 0.2 cm in height. A saturated solution of ethanol and lithium hydroxide (LiOH) was prepared. An electrochemical cell was prepared by submerging the pellet into an electrochemical cell using the MoS₂ pellet as an electrode and the platinum counter electrode. A power supply was used to apply -5 V to the MoS₂ pellet for 5 h. After 5 h the pellet was removed and dried.

The lithium intercalated pellet was dispersed in a 50 mL mixed solvent of (3:7) IPA and water and placed into an ice bath. The mixture was tip sonicated with a Cole-Parmer CP-130 Ultrasonic Processor (30% of 130W and 20Khz) with a pulse setting of 7s on 10s off and maintaining a temperature below 30°C. After 1 h the mixture was centrifuged at 3500 rpm for 20 min and the supernatant was collected and stored for the composite preparation. Additional exfoliated MoS₂ suspension was obtained from the deposited material. This unsuspended material was collected and mixed again with 25mL of deionised water and IPA (7:3) and sonicated with the same parameters. This procedure was repeated once more.

Synthesis of GO:

GO was synthesised using a modified Hummers method.⁹⁵

7.5g of bulk graphite was mixed with 360 mL H₂SO₄ in an ice bath with magnetic stirring, 15g of KMnO₄ was added slowly and left for 10 min. The resulting solution was subjected to microwave treatment for 10 min at 250W, then diluted with 1 L of ice. The resulting solution

was then cooled in an ice bath and 150 mL of H₂O₂ was added slowly with stirring. The solution was then centrifuged at 4000 rpm then washed with 2.4 L of 1 mol/L HCl solution to remove the Mn and left for 5 min. The solution was then centrifuged again and washed with deionised water until the pH reaches 7. The GO was suspended in 1.4 L of deionised water by sonicating at 60°C for 30 min. The suspension was centrifuged again, and the supernatant was collected.

Preparation of the rGO/MoS₂ aerogel:

3 mL of rGO suspension was mixed with 24 mg of ascorbic acid. The resulting mixture was sonicated for 20 mins to ensure a homogenous mixture and NH₄OH was added dropwise until the solution was pH ~10. The mixture was heated for 2 hrs at 95°C. After 2 h the resulting hydrogel was frozen in a conventional refrigerator freezer (~-18°C) for 2 hours and submitted to more 2 h heating at 95°C. Then, left in a 1:100 solution of water and ethanol for 5 h for dialysis. The resulting hydrogel monolith was frozen once more for 5 h to promote formation of pores and left to dry in ambient conditions. The resulting aerogel was collected and cut to around 1 cm in length and 0.3 cm in width. The rGO/MoS₂ aerogel was prepared by immersing the aerogel in the MoS₂ suspension for 30 min and dried in ambient conditions.

Electrochemical characterisation (supercapacitor application):

The electrochemical properties were investigated by cyclic voltammetry (CV), galvanostatic charge-discharge (GCD) and electrochemical impedance spectroscopy (EIS) using an electrochemical workstation (Bio-logic vmp3). All tests were conducted using a three-electrode flooded cell in a 1M solution of Li₂SO₄. The rGO/MoS₂ aerogel was used as the negative electrode while a platinum plate (5 cm²) was the counter electrode. Ag|AgCl|KCl_(sat) was used as a reference electrode.

Raman:

This technique was used to study the vibrational modes of exfoliated MoS₂. The characterisation was carried out between the wavenumber 0 to 1000 cm⁻¹. The excitation laser was at the wavelength 488 nm. This was carried at CTNANO UFMG. The bulk and exfoliated material were both characterised for comparison. Both materials were deposited on a quartz block.

Scanning Electron Microscopy:

This technique was used to gain detailed morphological features of exfoliated MoS₂ as well as the rGO/MoS₂ aerogel composite. Scanning electron microscopy (SEM) was used to observe the aggregation of MoS₂ after exfoliation. Elemental mapping was used to distinguish the regions of the composite aerogel that has aggregation of MoS₂. SEM was performed at the Centro de Microscopia da UFMG (UFMG Microscopy Centre). All samples were deposited onto a carbon tape for characterisation.

Preparation of an MoS₂ gas sensor:

A thin film of MoS₂ was prepared on a glass slide by spray coating. Once dried silver paint was applied at two edges and a digital multi-meter was attached to measure the change in resistance.

Preparation of and microfiber cellulose/MoS₂ composite gas sensor:

33 mL of MoS₂ suspension was mixed with 67 mL of suspended microfiber cellulose (MFC) and bath sonicated for 10 min. A thin film of microfiber cellulose/MoS₂ was prepared on a glass slide by spray coating. A dried silver paint was applied at two edges and a digital multi-meter was attached to measure the change in resistance.

6. Results and Discussion

8.1 Exfoliation of MoS₂ with IPA and water

In order to avoid solvents such as NMP and DMF, a mixed solvent of an alcohol and water was used. IPA presents a far less risk to the environment and is far less toxic. This work along with other recent studies found that IPA is a valid solvent for exfoliating MoS₂.⁹⁶⁻⁹⁹ Mixed solvent systems like that used in this study have been investigated theoretically.⁴⁰ Our studies aim to a more solid empirical basis as the investigation of the differing mixtures of IPA and water with the changing sonication parameters give an overview of the more effective mixtures for exfoliating MoS₂ and help to give the use of mixed solvent systems more validity.

This study was set up to test different parameters in steps: step 1) IPA concentration; step 2) Time of exfoliation; and step 3) amplitude of sonication. The study was set up as a process of elimination where the experimental condition that yielded the superior result was carried forward to the next step.

Initially tip sonication was carried out in a solution of varying IPA concentrations to evaluate the effect on particle size in suspension. Fig. 13. shows the DLS results for the colloidal suspensions of MoS₂ with these varying concentrations. Fig 11. A shows a good distribution of MoS₂ sizes, with an average hydrodynamic diameter of 282 nm as shown in table 2. Fig. 11. B shows a similar distribution; however, it is shifted to the right. The average particle size for this distribution is larger with an average size of 450.7 nm. Finally, Fig. 13. C shows the results for the 4:6 IPA:Water ratio. This result is the poorest distribution as the particles are very polydisperse as a suspension where the majority of particles are in a narrow size range is preferable. This change can be attributed to the changing properties of the solvent as the IPA and water are mixed in closer amounts. These results indicate that the ratio of 3:7 is the best and therefore this ratio will be carried forward and the others abandoned.

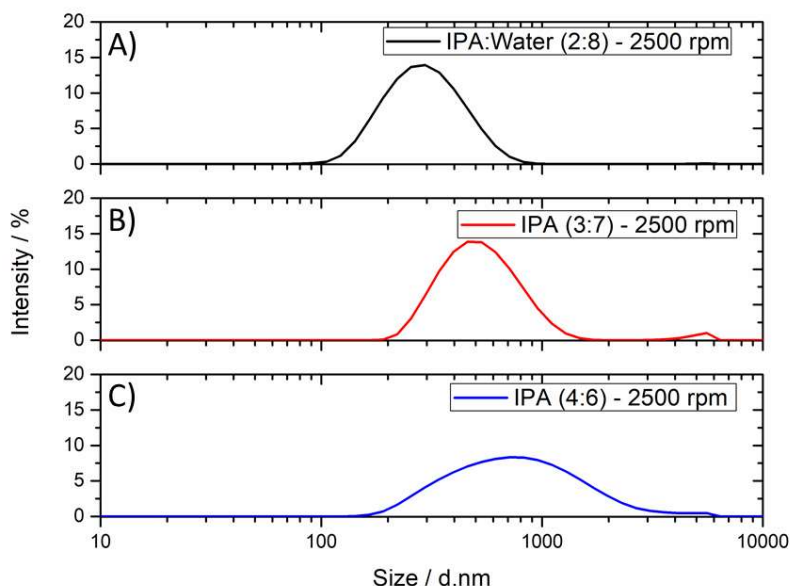


Fig. 13. DLS results for various IPA concentrations in water for MoS₂ exfoliation. IPA:Water ratio: A) 2:8, B) 3:7 e C) 4:6.

IPA:Water ratio	Average particle diameter (nm)
2:8	282
3:7	450.7
4:6	752.2

Table 2. Average particle size for all IPA concentrations studied.

Next the effect of sonication time was investigated. Since in the previous study 3:7 gave the best result this parameter was used throughout the time of sonication study. Since in the previous study 3x1 h sonication treatments were performed, in this step a series of 3x2 h treatments and 3x3 h treatments were performed. Since 3x1 h was performed in the previous step I was not repeated. The longer sonication time appeared to have a negative effect on the quality of the suspension. Both Fig. 14. A&B show that the average particle size has decreased (see also table 3), Fig. 14. B shows a much larger distribution of MoS₂ particles. This can be attributed to the fact that at longer sonication times the bulk MoS₂ will begin to break apart forming many smaller particles, this can be easily seen at the smaller end of the distribution. Both Fig. 14 A&B show peaks at around 1-10 μm. Since sonication will produce a lot of heat energy, this will promote random collisions in the suspension and will cause the agglomeration of large particles. Since the increase of sonication time overall caused a decrease in particle size and an increase in polydispersity it was concluded that that 3x1 h is the better procedure and was carried forward.

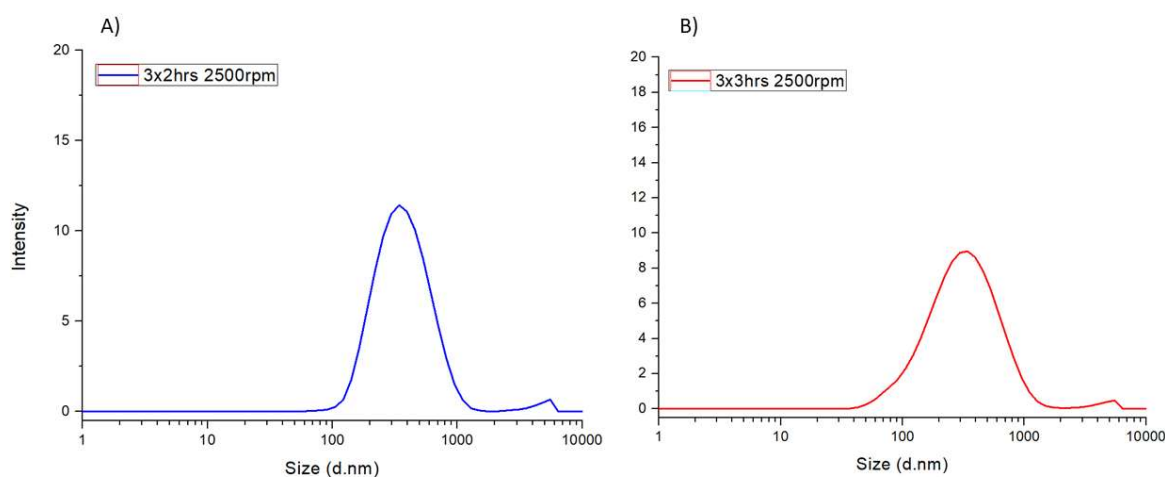


Fig. 14. DLS results for various sonication times for MoS₂ exfoliation. A) used a sonication time of 3x2 h B) used 3x3 h

Sonication time	Average particle diameter (nm)
3x1 h (step 1 test)	450.7
3x2 h	347.7
3x3 h	327.5

Table 3. Average particle size for all sonication times studied.

The final exfoliation parameter tested was the amplitude of the sonication tip, the ultrasonic bath was also utilised in this test for means of comparison. Fig. 15 shows the DLS results of the differing conditions. The bath sonication gives the largest particle sizes and largest distribution. Fig. 15. B&C give similar results, 20% amplitude gave smaller average particle sizes, this can be attributed to the lower sonication intensity being too low to suspend and exfoliate larger particles from the bulk material. This issue seems to be addressed by the 30% amplitude tip sonication.

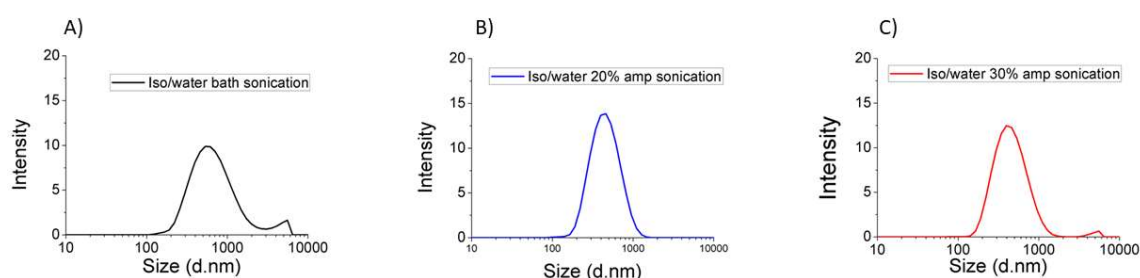


Fig. 15. DLS results for varying sonication amplitudes A) is bath sonication B) tip sonication at 20% C) tip sonication at 30%

Exfoliation method	Average particle diameter (nm)
Ultrasonic Bath	605.0
Tip Sonication (20% amplitude)	416.0
Tip Sonication (30% amplitude)	420.6

Table 4. Average particle size for sonication amplitudes.

The differences between these parameters was further investigated by performing AFM. Fig. 16. A shows the large exfoliated particles obtained via bath sonication, the height profile show that the MoS₂ crystal has a height of 0.9 nm which indicates that monolayers have been obtained. However, the intense heat and rigorous turbulence produced in the bath sonication process has caused holes to form in the interior of the nanosheet. This will cause a massive

decrease in the nanosheets strength and will disrupt its electrical properties. Fig. 16. B is the AFM image of the nanomaterial produced with a 20% amp of tip sonicator, the many small particles are due to the weaker intensity not exfoliating larger particles, the height profile shows 2.65 nm which is around 3-4 layers. Therefore, this amplitude is unable to suspend large particles and effectively exfoliate the MoS₂. Fig. 16. C is the 30% amp AFM image, this demonstrates that 30% amp is able to suspend large particles and effectively exfoliate MoS₂. The height profile shows a crystal height of 1.1 nm corresponding to 1 to 2 layers.

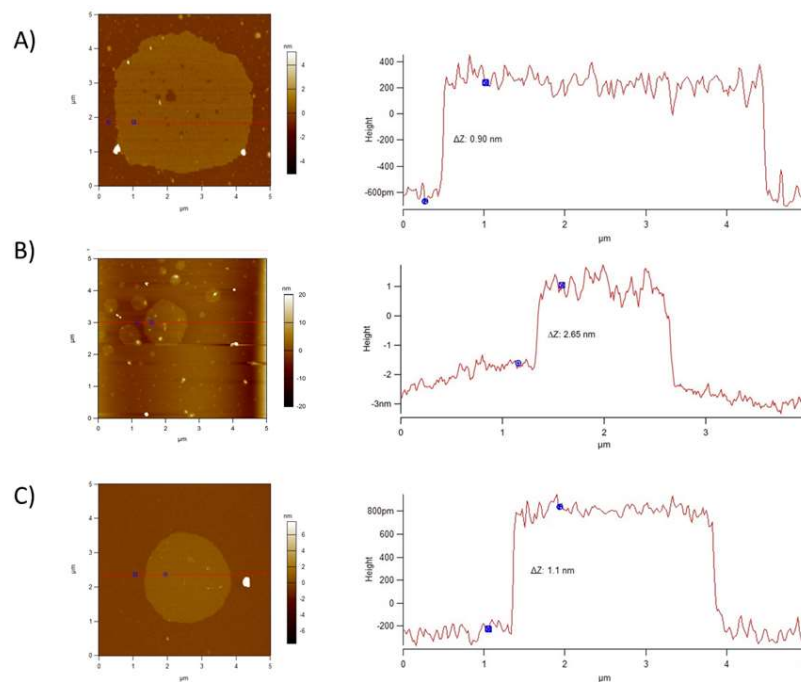


Fig. 16. AFM images of exfoliated MoS₂ A) MoS₂ exfoliated by bath sonication B) 20% amp tip sonication C) 30% amp tip sonication

The DLS results combined with the AFM images show that tip sonication with 30% amplitude is the ideal intensity for exfoliating MoS₂.

Fig. 17 shows TEM images of the exfoliated MoS₂ where the morphology of the MoS₂ nanosheets can be seen, Fig. 17 A&B are images of nanomaterials produced by the bath sonication and E&F by the 30% tip sonication. The few layers can be seen as the transparency is clear indicating that the TEM electron beam is encountering few layers of material. Fig. 17 C&D are the images of the 20% tip sonication, in image D the layers of MoS₂ can be clearly seen.

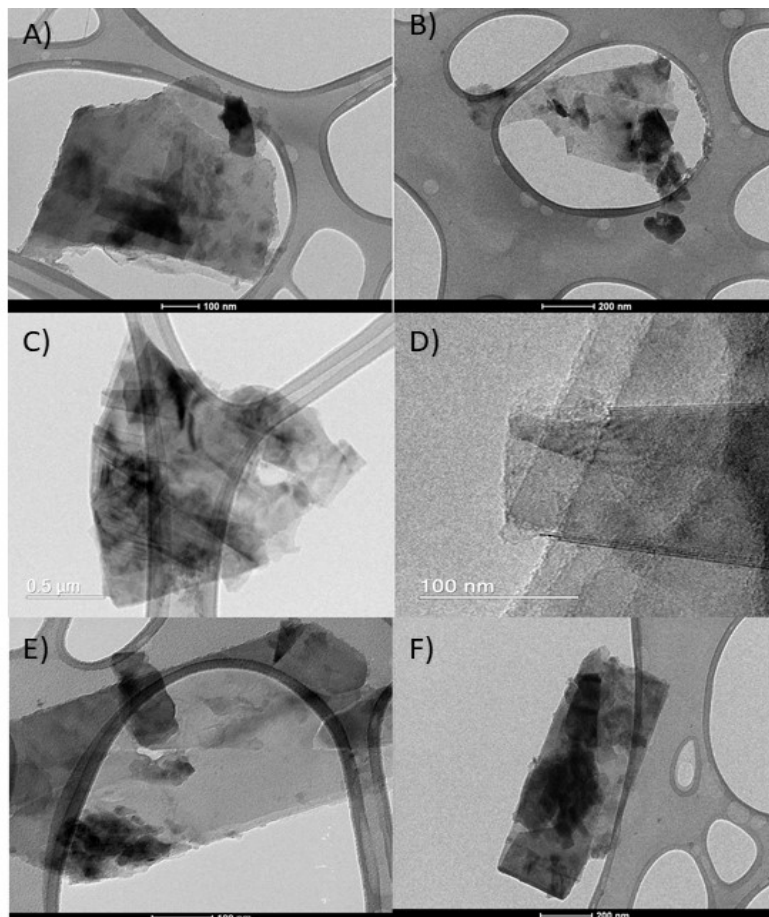


Fig. 17. TEM images of exfoliated MoS₂ A&B) bath sonication C&D) 20% tip sonication E&F) 30% tip sonication

The results indicate that the ideal exfoliation process is mixing MoS₂ in 3:7 IPA:Water mixed solvent, tip sonicating at 30% amplitude for 3x1 h. Table 5 shows a comparison of the results obtained in this work with that found in the literature.

Fig. 18 shows the SAED results for MoS₂ obtained using 30% tip sonication, the pattern is indicative of 2H-MoS₂ and the lack of rings in the diffraction pattern are due to monolayer formation.⁵³

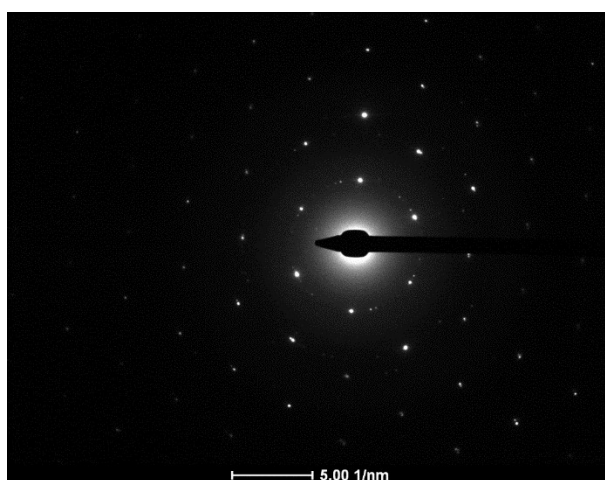


Fig. 18 TEM SAED image of MoS₂ produced by 30% amplitude tip sonication.

Method	Solvent	Additive	Exfoliation time (h)	Average size (nm)	Average number of layers	Ref
LPE – Mechanical	H ₂ O	None	1	242	5	100
LPE – Sonication (Tip)	IPA	Salts	2	200-750	<4	57
LPE – Sonication (Tip)	H ₂ O:IPA 3:7	None	4	200-750	<4	101
LPE – Sonication (Tip)	Hexane	BuLi	1.5	300	<4	44
LPE – Shear	Water/Ethanol (45%)	None	1-10	200-6000	<4	37
LPE – Sonication (Bath)	NMP	NaOH	2	50-1000	1-9	102
LPE – Sonication (Tip)	DMF	None	5	3000-20000	1-10	103
LPE – Sonication (Tip)	IPA:H ₂ O 3:7	None	3x1	450.7	<4	This work

Table 5. Comparison of exfoliation methods in the literature and this work

8.2 Intercalation of MoS₂ and preparation of supercapacitor electrode material:

Since the parameters for exfoliating MoS₂ have been established, it was necessary to investigate how it could be implemented into applications. The first of which was investigating MoS₂ nanosheets as a supercapacitor electrode material. Firstly it was necessary to develop a method for intercalating bulk MoS₂ with Li⁺ ions to induce a phase transition from 2H-MoS₂ to 1T-MoS₂¹³ as the MoS₂ will perform better in this phase as a supercapacitor material.^{85,86} However maintaining MoS₂ in the 1T phase its difficult as it will transition back to 2H-MoS₂ with heating and aging.¹⁹ Mahmood et al.¹⁰⁴ described how surfaces of rGO and MoS₂ in contact will stabilise the 1T-MoS₂ phase. Therefore, an rGO/MoS₂ composite was used in this study.

A new method of intercalating Li^+ ions was investigated to avoid using organolithiums. This approach attempts to address these problems by using LiOH solubilised in ethanol. Ethanol was chosen as when performed in water, electrolysis of water inhibits the intercalation of Li^+ and the fast intercalation of Li^+ will cause considerable mass loss due to the pellet breaking. A pulse setting was used on the tip sonicator and the exfoliation was carried out in an ice bath to prevent a phase transition back to 2H-MoS_2 .

Evaporation of 100 mL of this obtained suspension it was determined that the concentration of 0.06 wt% or 0.06 mg/mL.

In Fig. 19 is an AFM image of MoS_2 after intercalation and exfoliation. The MoS_2 has a slightly different height profile, this can be attributed to the use of the ice bath and pulse sonication. The height profile indicates 2-3 layers, therefore, very few layers are still obtained.

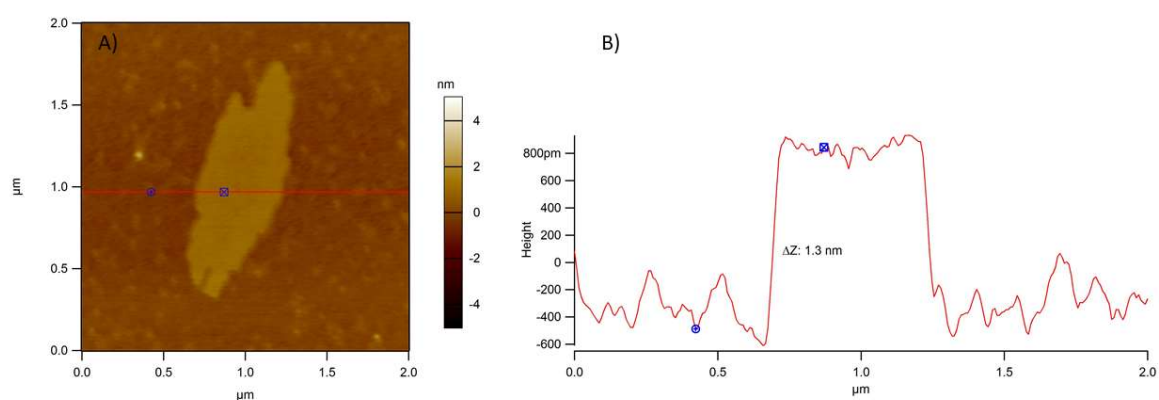


Fig. 19. A) AFM of Li^+ intercalated and exfoliated MoS_2 B) Height profile of the AFM image

Fig. 19 shows the Raman spectra for bulk and exfoliated MoS_2 ; the bulk shows two bands the E_{2g}^1 is the in-plane mode at 380 cm^{-1} and the A_{1g} which is the out-plane mode at 406 cm^{-1} . The exfoliated material shows the E_{2g}^1 peak at 381 cm^{-1} and the A_{1g} peak is at 406 cm^{-1} . There has been a decrease in the distance between the peaks which indicates the layer number has decreased,¹⁰⁵ the wavenumber difference between the E_{2g}^1 and the A_{1g} in the bulk material is 26.1 cm^{-1} while this difference in the exfoliated material is 24.7 cm^{-1} this gives further evidence for the presence of few layers because the wavenumber difference of these peaks only becomes sensitive to change when the nanosheets are less than 4 layers.⁵⁷

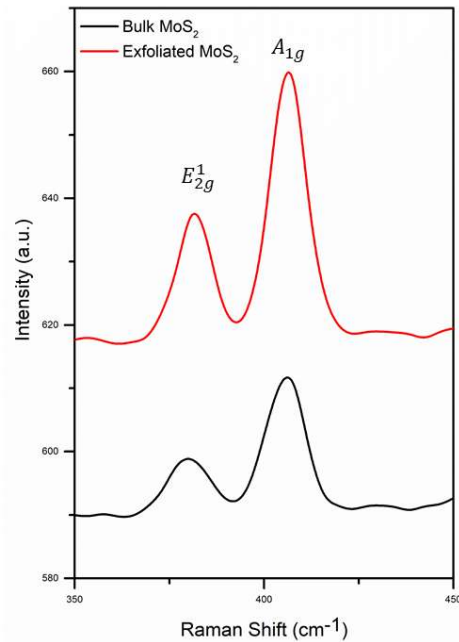


Fig. 20. Raman spectra of bulk MoS₂ and exfoliated MoS₂

When MoS₂ is deposited onto a material it has a tendency to agglomerate and restack as shown in Fig. 21. The nanosheets appear to stack together randomly in Fig. 21. Many small nanosheets can be seen along with many larger elongated MoS₂ crystals. This issue of restacking can be addressed by allowing the material to deposit onto a high surface area 3D object, such as an aerogel discussed below.

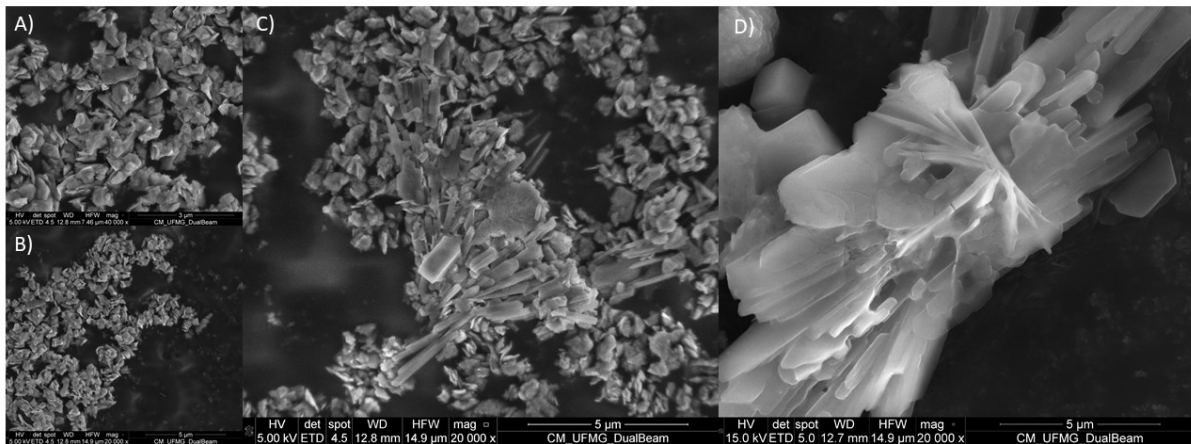


Fig. 21. A-D SEM images of exfoliated MoS₂.

An aerogel of rGO was synthesised as the highly porous nature of aerogels make them ideal for supercapacitors. In the initial step the pH of the GO suspension is adjusted to ~10; the higher pH will promote deprotonation of the functional groups on the GO surface and

reduction at this high pH will yield more efficient restoration of the sp^2 graphitic network¹⁰⁶. The GO and ascorbic acid were mixed and sonicated in an ultrasonic bath for 20 mins to ensure a homogeneous mixture, without such homogenisation the formed hydrogel and subsequent aerogel would be far less structurally stable and would collapse. Ascorbic acid was used as a reducing agent as it is environmentally friendly and will promote the self-assembly via crosslinking¹⁰⁷. After heating at 95°C for 2 h the hydrogel was removed and washed thoroughly with deionised water, this removed any rGO that did not form into the hydrogel. The hydrogel was left in a 1:100 mixture of water for 5hrs, the solvent exchange allowed the removal of any impurities especially the ascorbic acid. After these impurities were removed the hydrogel was left to dry to form the aerogel. Because of the sponge-like nature of the aerogel, it could be submerged into the MoS_2 suspension and the aerogel would soak up the MoS_2 suspension, depositing it on the rGO surface.

The issue of the MoS_2 agglomeration is addressed by the process dripping the suspension onto the rGO aerogel. Fig. 22. shows the SEM images of MoS_2 deposited onto the surface of the aerogel, MoS_2 deposits form homogeneous pockets throughout the aerogel surface, these regions are much smaller than that observed in the SEM images in Fig. 21. The fact that the regions of MoS_2 are more dispersed throughout the aerogel surface means that the likelihood of complete restacking of MoS_2 to the extent that it would resemble the bulk material is significantly reduced. Fig. 22. D&E show a region of the aerogel with MoS_2 with elemental mapping, where the region of MoS_2 is only roughly $3\mu m$ across vs the much larger accumulation seen in the pure MoS_2 . Fig. 22. C shows the porosity of the rGO aerogel, its sponge-like nature can be fully seen. It appears that the aerogel forms small pores close to the centre and forms progressively larger pores towards the exterior. This large surface area is very conducive to the structure of an electrode designed to hold charge, there are many areas in which electrochemical interactions can occur.

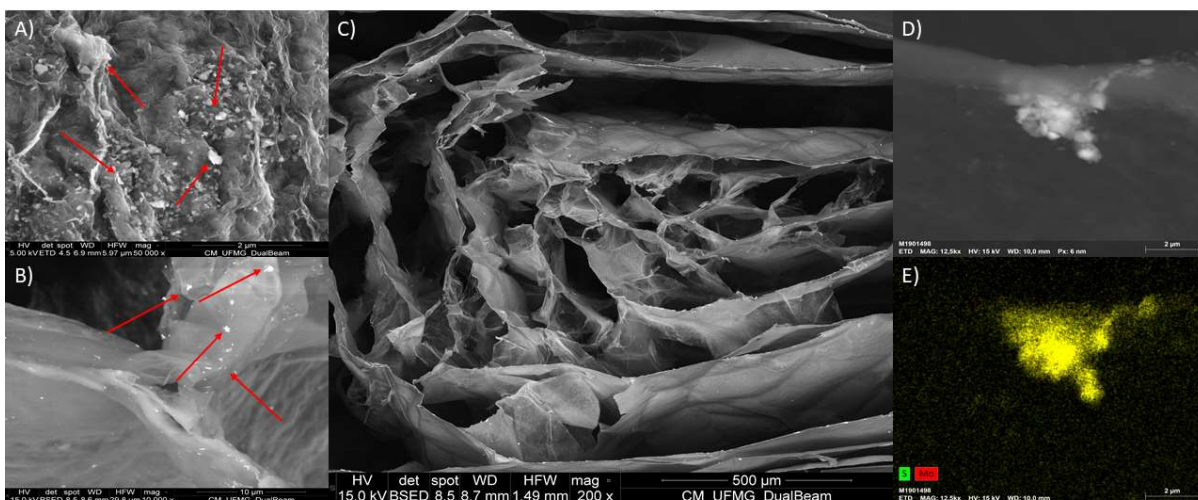


Fig. 22. (A & B) SEM back-scattering electron images with red arrows indicating deposits of MoS₂. (C) SEM image of the structure of the rGO/MoS₂ aerogel composite. (D&E) SEM image of a pocket of MoS₂ with elemental mapping.

The electrochemical characterisation was carried out in a half-cell set up, both the pure rGO and rGO/ MoS₂ aerogels were tested separately as working electrodes in an aqueous solution of 1M Li₂SO₄. These measurements were performed in a typical 3 electrode cell, by using a platinum counter-electrode and a Ag/AgCl/KCl reference electrode. Fig. 23 shows the cyclic voltammetry (CV) results for both the pure rGO aerogel electrode and the rGO/ MoS₂ aerogel electrode operating between -0.8 and 0 V at a fixed scan rate of 5 mV s⁻¹. Between -0.7 and 0 V the CV profiles for both rGO electrode and the composite have a rectangular or box-shaped, indicating the formation of an electric double layer as the principal charge storage mechanism, the increase of current that appears at -0.8 V in both profiles is much more pronounced in the composite electrode. This region can be attributed to the water electrolysis due to MoS₂ promoting catalytic hydrogen evolution¹⁰⁸. Since the energy storage process is related to the area within the CV box, one can observe that the rGO/MoS₂ aerogel composite was significantly improved over the pure rGO aerogel electrode.

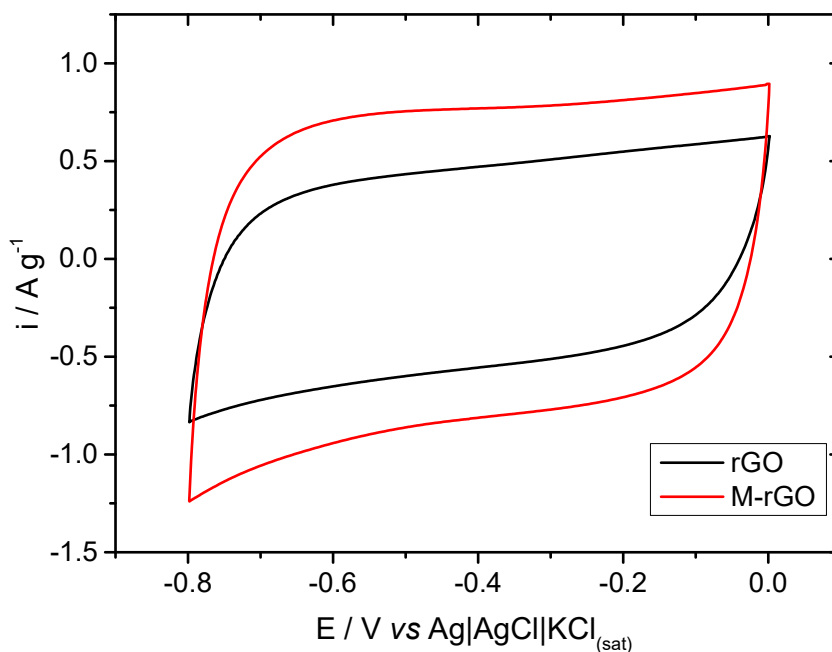


Fig. 23. CV plot between -0.8 and 0 V at 5 mV S^{-1}

The charge-discharge curves, shown in Fig. 24. A&B were used to investigate the capacitance and to understand the charge storage mechanism. The triangular shape of the charge-discharge plot gives further evidence for the charge storage mechanism being electric double-layer. Both plots show that the charge-discharge time is faster at higher current rates and visa versa. This is because at lower current densities the electrolyte ions have enough time to interact with the active sites.¹⁰⁹ The specific capacitance of both electrodes was calculated using the following equation:¹¹⁰

$$C_{sp} = \frac{2i \int V dt}{mV^2}$$

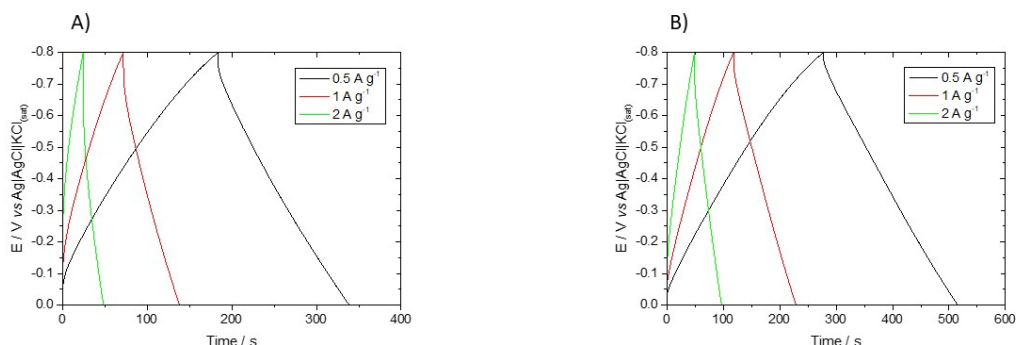


Fig. 24. Galvanostatic charge-discharge plots of electrochemical cell with electrodes of A) rGO aerogel and B) rGO/ MoS₂ aerogel

The calculated results from the charge-discharge plots in Fig. 25. A&B indicates that the addition of MoS₂ nanosheets has increased significantly the capacitance. At 0.5 A g⁻¹ the capacitance of the rGO/ MoS₂ aerogel was 140.4 F g⁻¹ vs the rGO aerogels capacitance of 87.4 F g⁻¹ (an increase of 62%). This increase can be attributed by the addition of MoS₂, Jiang et. al.¹¹¹ have reported that this improved electrochemical performance of rGO/MoS₂ composites is due to strong synergetic effects between the MoS₂ nanosheets and graphene nanosheets. The high coulombic efficiency indicates that the interactions at the electrode are reversible, Saraf et. al.¹¹² attribute this improved efficiency to composites of rGO and MoS₂ forming robust 2D heterostructures.

Current density / A g ⁻¹	rGO aerogel		MoS ₂ -rGO aerogel	
	C / F g ⁻¹	ε / %	C / F g ⁻¹	ε / %
0.5	87.4	84.5	140.4	85.2
1	73.7	92.8	130.6	93.7
2	53.4	95.1	113.2	98.5

Table 6. Table of the calculated values of capacitance (C) and coulombic efficiency (ε) for electrochemical cell with electrodes of rGO and MoS₂-rGO.

The cycling process and the retention capacity was studied by performing 5000 successive cycles, as shown in Fig. 25. A. These results indicate a high capacity retention with only 25%

of capacity fading upon the several cycles. In comparison Gao et al.¹¹³ found that pure MoS₂ nanosheets lost 25% of its initial capacity (129.2 F g⁻¹) after only 500 cycles at 1 A g⁻¹.

The EIS Fig. 25. B was measured in the frequency range from 100 kHz to 10 mHz. The plot shows a nearly vertical line at higher frequencies as the plot of an ideal supercapacitor would, where the arc at low frequencies is due to charge transfer resistance. Fig. 25 Shows that the rGO/ MoS₂ performs very well as an electrode material, it has good cyclability as the capacitance only drops slightly after 5000 cycles at 2 A g⁻¹

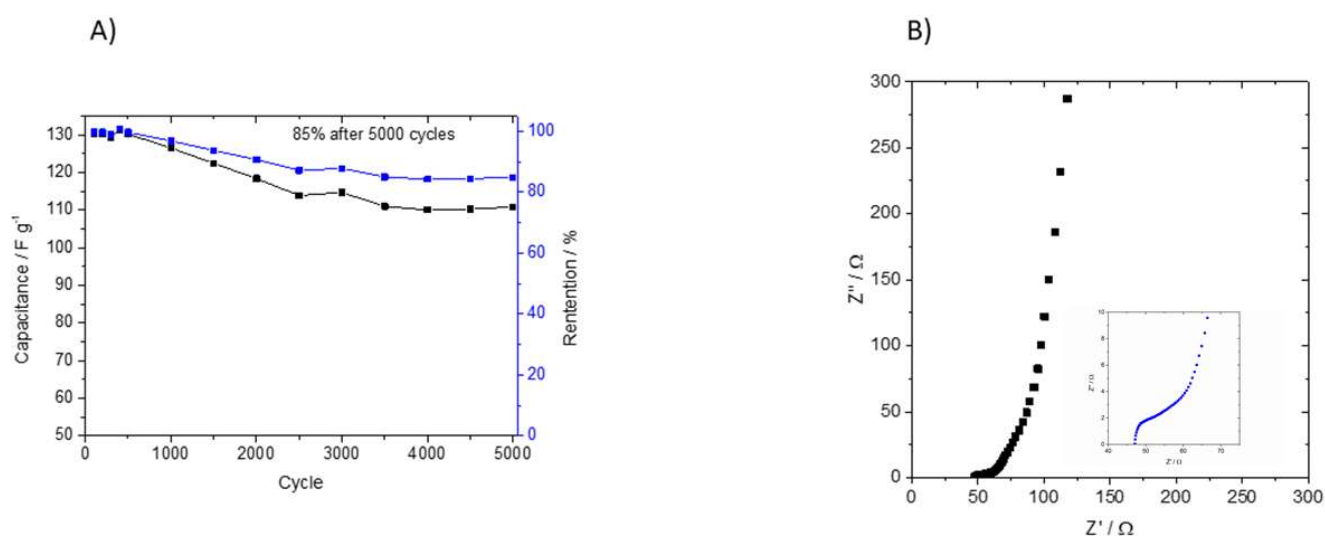


Fig. 25. Results for electrochemical cell with for rGO/MoS₂ electrode: A) capacitance and coulombic efficiency from 1 to 5000 cycles at 2 A g⁻¹ and B) The Nyquist plot electrode between 0.001 and 1000000 Hz.

In summary, an electrode material was developed using a composite of MoS₂ and rGO. The electrode material exhibits great capacitance at 140.4 F g⁻¹ at 0.5 A g⁻¹ and shows great cyclability maintaining 85% efficiency after 5000 cycles. Huang et al.¹¹⁴ found a similar improvement of capacitance with a graphene MoS₂ composite, the group found that at 1 A g⁻¹ MoS₂ and graphene alone gave 120.35 F g⁻¹ respectively. However, as a composite this capacitance rose significantly to 243 F g⁻¹ this is larger than the capacitance seen in the supercapacitor material studied in this work, this can be attributed to the use of graphene instead of rGO. Graphene can have a specific capacitance up to three times higher than rGO¹¹⁵. Therefore, this can be considered to further improve this electrode material in the future. Jung et al.¹¹⁶ studied the effect of controlling the porous structures of graphene

aerogels. The group was able to produce meso and macroporous graphene aerogels and this material exhibited a high specific 325 F g^{-1} . A similar procedure combined with MoS_2 could potentially produce an enhanced supercapacitor material.

8.3 Preparation of an MoS_2 based gas sensor:

MoS_2 was prepared as a thin film of $\sim 1\text{-}2 \mu\text{m}$ by spray coating to assess its capability as a gas sensor, specifically as a vapour sensor. Water vapour was passed across the surface of the thin film to record changes in the materials resistance. Both pure exfoliated MoS_2 and a composite of MFC/ MoS_2 was evaluated. The MFC was introduced with the goal of evaluating the effect of a highly hydrophilic material and how this will impact MoS_2 's performance as a gas sensor. The composite was made up of 33 mL of MoS_2 suspension (0.06 mg/mL) and 66 mL 0.1 wt/vol\% of MFC suspension. Fig. 26. shows the morphology of the MFC/ MoS_2 thin film. The fibres can be clearly seen in fig. 26 A.

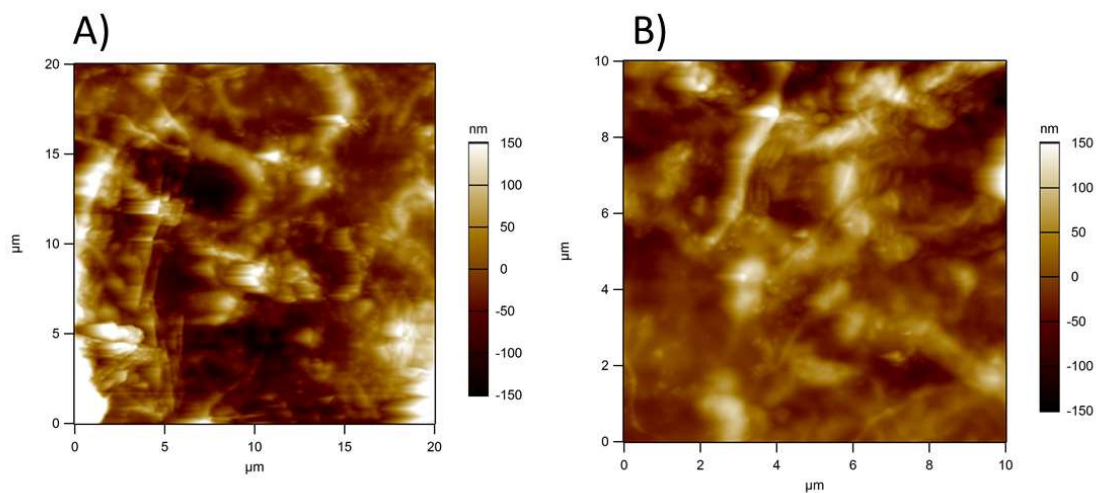


Fig. 26. AFM image of the morphology of the MoS_2 sensor

Fig. 27 shows an SEM image of the MFC/ MoS_2 composite, the MoS_2 is uniformly deposited on the MFC, this may improve the sensor's ability to detect water as it is easier for the water to bridge across each region of MoS_2 much more readily

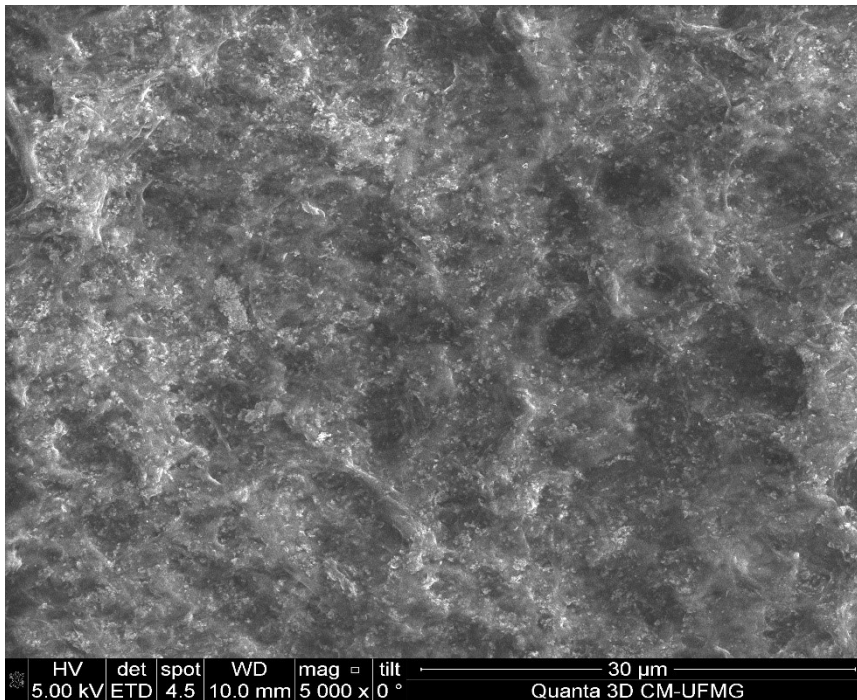


Fig. 27. SEM image of the sensor surface.

A thin film of exfoliated MoS₂ was first tested, it can be seen in Fig. 28 that $\Delta R/R_0$ is negative, therefore as the MoS₂ thin film is exposed to water vapour its conductivity increases. The response is very rapid in both plots in Fig. 28 exposure to water vapour will reach its maximum response at 4 s in the MoS₂ film and 3 seconds in the composite, the sensor will also return to its baseline resistivity in both cases ~10 s. The composite of MFC/MoS₂ gives a smoother curve and did not plateau in certain regions as seen with the pure MoS₂ thin film.

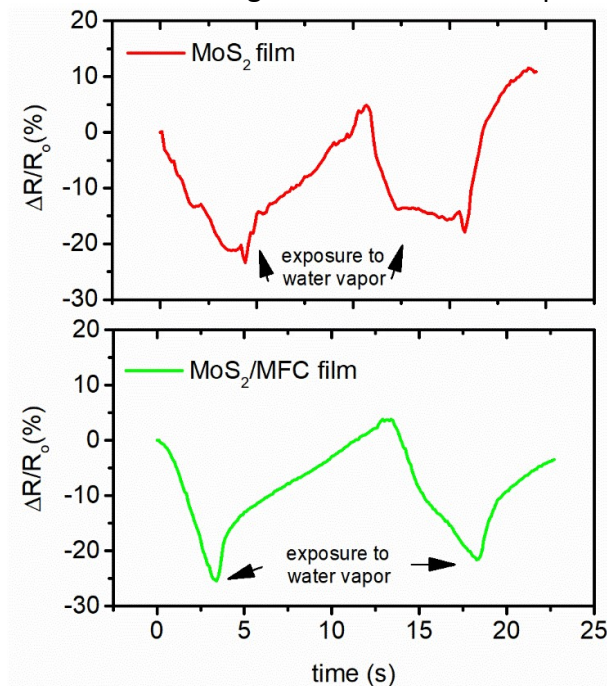


Fig. 28. Change is resistance vs time of both MoS₂ film and the composite under exposure to water vapour

Zhao et al.¹¹⁷ constructed a single layer MoS₂ based field effect transistor for humidity sensing. The sensor produced by the group would increase in resistivity with exposure to water in converse to what was observed with the sensor constructed in this work. This sensor had a much slower response to humidity, the time to reach maximum response was 10 s and it's time to decay back to its original resistivity was 50 s. However, the sensor was very sensitive to the relative humidity, with the device's on/off ratios decreasing linearly with varying the humidity from 0 to 35%. In contrast Li et al.¹¹⁸ studied at MoS₂/Ag thin film composite what had a response time of 1.5 s and was able to respond to relative humidity of 11-97% this was reported to be 22 times more sensitive than a pure MoS₂ thin film.

The composite thin film was also put into a closed container and N₂ was pumped into the container to evaluate its effect on the resistivity. Fig. 27 shows the effect of exposing the sensor to nitrogen gas, the resistivity increases. This can be attributed to the nitrogen forcing the water to desorb from the surface. The thin film quickly recovers back to baseline.

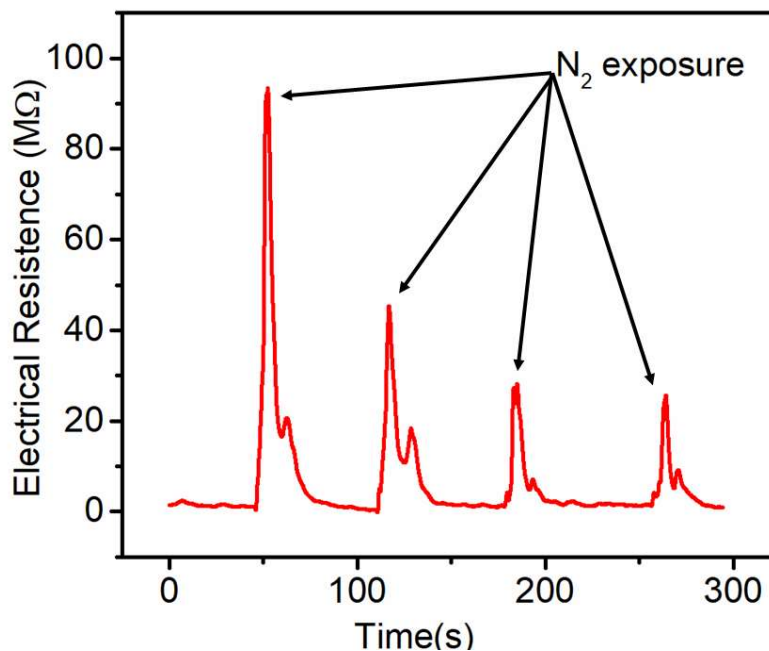


Fig. 29. Electrical resistance vs time with nitrogen exposure

In summary, a new method for detecting water vapour using a thin film of MCF/MoS₂ was developed, this thin film will become more conductive in the presence of water. The same composite also will quickly become resistant when exposed to N₂ and can potentially detect this gas.

7. Conclusions:

In conclusion of this work a new method for exfoliating MoS₂ was developed. The work aimed to find a greener way to suspend and exfoliate MoS₂ into few-monolayer nanosheets to counter the use of toxic and environmentally harmful solvents. This method was developed by systematically testing and adjusting each parameter involved in the liquid phase exfoliation process. It was determined that IPA and water are good solvents for exfoliating MoS₂ as the mixed solvent may have a much less harmful effect on the environment and a lower risk to health. After experiments in adjusting parameters, it was found that the best ratio of IPA to water is 3:7, the best time for exfoliation was 3x1 hrs and the best amplitude of tip sonication was 30% of 130 W and 20 KHz. DLS found that the average particle size with these parameters was 420 nm in diameter, and AFM showed around 1.1 nm of thickness (1-2 layers).

After developing this method, it was possible to explore two applications. First, a composite material for electrode of a supercapacitor that improves its electrochemical performance. The supercapacitor material composite was made of an rGO aerogel and exfoliated MoS₂, this electrode material had a very good capacitance of 140.4 F g⁻¹ at 0.5 A g⁻¹ and would maintain 85% of its initial capacitance after 5000 cycles. This improvement to the rGO aerogel capacitance of 87.4 F g⁻¹ can be attributed to the improved specific surface area with the addition with the addition of exfoliated MoS₂ and the improved ion diffusion facilitated by MoS₂. However, the measurements of specific surface area and diffusion coefficient will be made in further works.

A vapour sensor was also developed that allowed for the detection of water vapour. This sensor had a very fast response time when compared with a sensor based on a field effect transistor,¹¹⁸ rGO/MoS₂ based sensors¹¹⁹ and especially pure MoS₂ sensor.¹²⁰ The sensor incorporated exfoliated MoS₂ and MFC. This sensor would use a thin film that would become 25% more conductive when exposed to water vapour.

The process and applications studied in this work show potential. MoS₂ possess very interesting electrochemical properties and can spearhead material development for energy and electronic devices of the future

8. References:

1. Novoselov, K. S. *et al.* Electric field in atomically thin carbon films. *Science* (80-.). (2004). doi:10.1126/science.1102896
2. Manzeli, S., Ovchinnikov, D., Pasquier, D., Yazyev, O. V. & Kis, A. 2D transition metal dichalcogenides. *Nature Reviews Materials* (2017). doi:10.1038/natrevmats.2017.33
3. Samadi, M. *et al.* Group 6 transition metal dichalcogenide nanomaterials: Synthesis, applications and future perspectives. *Nanoscale Horizons* (2018). doi:10.1039/c7nh00137a
4. *Key World Energy Statistics 2016*. (2016). doi:10.1787/key_energ_stat-2016-en
5. Chang, K. & Chen, W. L -Cysteine-assisted synthesis of layered MoS₂/graphene composites with excellent electrochemical performances for lithium ion batteries. *ACS Nano* (2011). doi:10.1021/nn200659w
6. Pazhamalai, P., Krishnamoorthy, K., Manoharan, S. & Kim, S. J. High energy symmetric supercapacitor based on mechanically delaminated few-layered MoS₂ sheets in organic electrolyte. *J. Alloys Compd.* (2019). doi:10.1016/j.jallcom.2018.08.203
7. Novoselov, K. S. *et al.* Two-dimensional gas of massless Dirac fermions in graphene. *Nature* (2005). doi:10.1038/nature04233
8. Wilson, J. A. & Yoffe, A. D. The transition metal dichalcogenides discussion and interpretation of the observed optical, electrical and structural properties. *Adv. Phys.* (1969). doi:10.1080/00018736900101307
9. Hornyak, G. L. & Rao, A. K. Fundamentals of Nanoscience (and Nanotechnology). in *Nanoscience in Dermatology* (2016). doi:10.1016/B978-0-12-802926-8.00002-1
10. Zhang, H. Ultrathin Two-Dimensional Nanomaterials. *ACS Nano* (2015). doi:10.1021/acsnano.5b05040
11. Zheng, C., Zhou, X., Cao, H., Wang, G. & Liu, Z. Synthesis of porous graphene/activated carbon composite with high packing density and large specific surface area for supercapacitor electrode material. *J. Power Sources* (2014). doi:10.1016/j.jpowsour.2014.01.056
12. Zhang, Y. *et al.* Langmuir films and uniform, large area, transparent coatings of chemically exfoliated MoS₂ single layers. *J. Mater. Chem. C* (2017). doi:10.1039/c7tc02637d
13. Xia, J. *et al.* Phase evolution of lithium intercalation dynamics in 2H-MoS₂. *Nanoscale* (2017). doi:10.1039/c7nr02028g
14. Molina-Sánchez, A. & Wirtz, L. Phonons in single-layer and few-layer MoS₂ and WS₂. *Phys. Rev. B - Condens. Matter Mater. Phys.* (2011). doi:10.1103/PhysRevB.84.155413
15. Gusakova, J. *et al.* Electronic Properties of Bulk and Monolayer TMDs: Theoretical Study Within DFT Framework (GVJ-2e Method). *Phys. Status Solidi Appl. Mater. Sci.* (2017). doi:10.1002/pssa.201700218

16. Kobayashi, K. & Yamauchi, J. Electronic structure and scanning-tunneling-microscopy image of molybdenum dichalcogenide surfaces. *Phys. Rev. B* (1995). doi:10.1103/PhysRevB.51.17085
17. Splendiani, A. *et al.* Emerging photoluminescence in monolayer MoS₂. *Nano Lett.* (2010). doi:10.1021/nl903868w
18. Acerce, M., Voiry, D. & Chhowalla, M. Metallic 1T phase MoS₂ nanosheets as supercapacitor electrode materials. *Nat. Nanotechnol.* (2015). doi:10.1038/nnano.2015.40
19. Jiménez Sandoval, S., Yang, D., Frindt, R. F. & Irwin, J. C. Raman study and lattice dynamics of single molecular layers of MoS₂. *Phys. Rev. B* (1991). doi:10.1103/PhysRevB.44.3955
20. Enyashin, A. N. *et al.* New route for stabilization of 1T-WSe₂ and MoS₂ phases. *J. Phys. Chem. C* (2011). doi:10.1021/jp2076325
21. Enyashin, A. N. & Seifert, G. ELECTRONIC PROPERTIES OF MoS₂ MONOLAYER AND RELATED STRUCTURES. *Nanosyst. PHYSICS, Chem. Math.* (2014).
22. Grayfer, E. D., Kozlova, M. N. & Fedorov, V. E. Colloidal 2D nanosheets of MoS₂ and other transition metal dichalcogenides through liquid-phase exfoliation. *Advances in Colloid and Interface Science* (2017). doi:10.1016/j.cis.2017.04.014
23. O'Neill, A., Khan, U. & Coleman, J. N. Preparation of high concentration dispersions of exfoliated MoS₂ with increased flake size. *Chem. Mater.* (2012). doi:10.1021/cm301515z
24. Yuan, H. *et al.* High efficiency shear exfoliation for producing high-quality, few-layered MoS₂ nanosheets in a green ethanol/water system. *RSC Adv.* (2016). doi:10.1039/c6ra15310k
25. Zhang, S. *et al.* Wafer-scale transferred multilayer MoS₂ for high performance field effect transistors. *Nanotechnology* (2019). doi:10.1088/1361-6528/aafe24
26. Backes, C. *et al.* Guidelines for exfoliation, characterization and processing of layered materials produced by liquid exfoliation. *Chemistry of Materials* (2017). doi:10.1021/acs.chemmater.6b03335
27. Cunningham, G. *et al.* Solvent exfoliation of transition metal dichalcogenides: Dispersibility of exfoliated nanosheets varies only weakly between compounds. *ACS Nano* (2012). doi:10.1021/nn300503e
28. Hildebrand, J. H.; Prausnitz, J. M.; Scott, R. L. *Regular and Related Solutions*, 1st ed.; Van Nostrand Reinhold Company: New York, (1970); p 228.
29. Hernandez, Y. *et al.* High-yield production of graphene by liquid-phase exfoliation of graphite. *Nat. Nanotechnol.* (2008). doi:10.1038/nnano.2008.215
30. Guardia, L. *et al.* Production of aqueous dispersions of inorganic graphene analogues by exfoliation and stabilization with non-ionic surfactants. *RSC Adv.* (2014). doi:10.1039/c4ra00212a
31. Yadav, S. *et al.* Facile synthesis of molybdenum disulfide (MoS₂) quantum dots and its application in humidity sensing. *Nanotechnology* (2019). doi:10.1088/1361-6528/ab1569

32. Jiang, F. *et al.* Use of organic solvent-assisted exfoliated MoS₂ for optimizing the thermoelectric performance of flexible PEDOT:PSS thin films. *J. Mater. Chem. A* (2016). doi:10.1039/c6ta00305b
33. Ghasemi, F. & Mohajerzadeh, S. Sequential Solvent Exchange Method for Controlled Exfoliation of MoS₂ Suitable for Phototransistor Fabrication. *ACS Appl. Mater. Interfaces* (2016). doi:10.1021/acsami.6b07211
34. Gan, X. *et al.* Covalent functionalization of MoS₂ nanosheets synthesized by liquid phase exfoliation to construct electrochemical sensors for Cd (II) detection. *Talanta* (2018). doi:10.1016/j.talanta.2018.01.059
35. Muscuso, L., Cravanzola, S., Cesano, F., Scarano, D. & Zecchina, A. Optical, vibrational, and structural properties of MoS₂ nanoparticles obtained by exfoliation and fragmentation via ultrasound cavitation in isopropyl alcohol. *J. Phys. Chem. C* (2015). doi:10.1021/jp511973k
36. Qi, Y. *et al.* A green route to fabricate MoS₂ nanosheets in water-ethanol-CO₂. *Chem. Commun.* (2015). doi:10.1039/c5cc00106d
37. Yuan, H. *et al.* High efficiency shear exfoliation for producing high-quality, few-layered MoS₂ nanosheets in a green ethanol/water system. *RSC Adv.* (2016).
38. Smith, R. J. *et al.* Large-scale exfoliation of inorganic layered compounds in aqueous surfactant solutions. *Adv. Mater.* (2011). doi:10.1002/adma.201102584
39. Ma, H., Shen, Z. & Ben, S. Understanding the exfoliation and dispersion of MoS₂ nanosheets in pure water. *J. Colloid Interface Sci.* (2018). doi:10.1016/j.jcis.2017.11.013
40. Zhou, G. *et al.* Molecular Simulation of MoS₂ Exfoliation. *Sci. Rep.* (2018). doi:10.1038/s41598-018-35008-z
41. Backes, C. *et al.* Functionalization of liquid-exfoliated two-dimensional 2H-MoS₂. *Angew. Chemie - Int. Ed.* (2015). doi:10.1002/anie.201409412
42. Kan, M. *et al.* Structures and phase transition of a MoS₂ monolayer. *J. Phys. Chem. C* (2014). doi:10.1021/jp4076355
43. Ambrosi, A., Sofer, Z. & Pumera, M. Lithium intercalation compound dramatically influences the electrochemical properties of exfoliated MoS₂. *Small* (2015). doi:10.1002/sml.201400401
44. Fan, X. *et al.* Fast and Efficient Preparation of Exfoliated 2H MoS₂ Nanosheets by Sonication-Assisted Lithium Intercalation and Infrared Laser-Induced 1T to 2H Phase Reversion. *Nano Lett.* (2015). doi:10.1021/acs.nanolett.5b02091
45. Zeng, Z. *et al.* Single-layer semiconducting nanosheets: High-yield preparation and device fabrication. *Angew. Chemie - Int. Ed.* (2011). doi:10.1002/anie.201106004
46. Lotya, M., Rakovich, A., Donegan, J. F. & Coleman, J. N. Measuring the lateral size of liquid-exfoliated nanosheets with dynamic light scattering. *Nanotechnology* (2013). doi:10.1088/0957-4484/24/26/265703
47. Badaire, S., Poulin, P., Maugey, M. & Zakri, C. In situ measurements of nanotube dimensions in suspensions by depolarized dynamic light scattering. *Langmuir* (2004). doi:10.1021/la049096r

48. Atkins, P. & Paula, J. De. Atkins' Physical chemistry 8th edition. *Chemistry* (2009). doi:10.1021/ed056pA260.1
49. Santos, S., Barcons, V., Christenson, H. K., Font, J. & Thomson, N. H. The intrinsic resolution limit in the atomic force microscope: Implications for heights of nano-scale features. *PLoS One* (2011). doi:10.1371/journal.pone.0023821
50. Cappella, B. & Dietler, G. Force-distance curves by atomic force microscopy. *Surf. Sci. Rep.* (1999). doi:10.1016/S0167-5729(99)00003-5
51. Schumacher, A., Scandella, L., Kruse, N. & Prins, R. Single-layer MoS₂ on mica: studies by means of scanning force microscopy. *Surf. Sci.* (1993). doi:10.1016/0039-6028(93)90875-K
52. Novoselov, K. S. *et al.* Two-dimensional atomic crystals. *Proc. Natl. Acad. Sci. U. S. A.* (2005). doi:10.1073/pnas.0502848102
53. Kaushik, V. *et al.* Scalable Exfoliation of Bulk MoS₂ to Single- and Few-Layers Using Toroidal Taylor Vortices. *Nanomaterials* (2018). doi:10.3390/nano8080587
54. Fultz, B. & Howe, J. M. *Transmission electron microscopy and diffractometry of materials. Transmission Electron Microscopy and Diffractometry of Materials* (2008). doi:10.1007/978-3-540-73886-2
55. Wu, R. J., Odlyzko, M. L. & Mkhoyan, K. A. Determining the thickness of atomically thin MoS₂ and WS₂ in the TEM. *Ultramicroscopy* (2014). doi:10.1016/j.ultramic.2014.05.007
56. Cai, Y., Lan, J., Zhang, G. & Zhang, Y. W. Lattice vibrational modes and phonon thermal conductivity of monolayer MoS₂. *Phys. Rev. B - Condens. Matter Mater. Phys.* (2014). doi:10.1103/PhysRevB.89.035438
57. Liu, H. *et al.* Production of mono- to few-layer MoS₂ nanosheets in isopropanol by a salt-assisted direct liquid-phase exfoliation method. *J. Colloid Interface Sci.* (2018). doi:10.1016/j.jcis.2018.01.023
58. Winter, M. & Brodd, R. J. What are batteries, fuel cells, and supercapacitors? *Chem. Rev.* (2004).
59. Horizon 2020: EU framework programme for research and innovation. *Int. J. Disaster Resil. Built Environ.* (2014). doi:10.1108/ijdrbe-03-2014-0023
60. Christen, T. & Carlen, M. W. Theory of ragone plots. *J. Power Sources* (2000). doi:10.1016/S0378-7753(00)00474-2
61. Wang, Y., Song, Y. & Xia, Y. Electrochemical capacitors: mechanism, materials, systems, characterization and applications. *Chem. Soc. Rev.* (2016). doi:10.1039/c5cs00580a
62. Roldán, S. *et al.* An approach to classification and capacitance expressions in electrochemical capacitors technology. *Phys. Chem. Chem. Phys.* (2015). doi:10.1039/c4cp05124f
63. Helmholtz, H. Ueber einige Gesetze der Vertheilung elektrischer Ströme in körperlichen Leitern mit Anwendung auf die thierisch-elektrischen Versuche. *Ann. Phys.* (1853). doi:10.1002/andp.18531650603
64. Zhang, L. L. & Zhao, X. S. Carbon-based materials as supercapacitor electrodes. *Chemical Society Reviews* (2009). doi:10.1039/b813846j

65. Hao, P. *et al.* High Performance Supercapacitors from Hierarchical Porous Carbon Aerogels Based on Sliced Bread. *Chinese J. Chem.* (2017). doi:10.1002/cjoc.201600722
66. Ali, G. A. M., Manaf, S. A. B. A., Kumar, A., Chong, K. F. & Hegde, G. High performance supercapacitor using catalysis free porous carbon nanoparticles. *J. Phys. D. Appl. Phys.* (2014). doi:10.1088/0022-3727/47/49/495307
67. Li, B. *et al.* Activated Carbon from Biomass Transfer for High-Energy Density Lithium-Ion Supercapacitors. *Adv. Energy Mater.* (2016). doi:10.1002/aenm.201600802
68. Hou, J., Cao, C., Idrees, F. & Ma, X. Hierarchical porous nitrogen-doped carbon nanosheets derived from silk for ultrahigh-capacity battery anodes and supercapacitors. *ACS Nano* (2015). doi:10.1021/nn506394r
69. Zhang, J. *et al.* Enhanced Performance of nano-Bi₂WO₆-Graphene as Pseudocapacitor Electrodes by Charge Transfer Channel. *Sci. Rep.* (2015). doi:10.1038/srep08624
70. Gujar, T. P., Kim, W. Y., Puspitasari, I., Jung, K. D. & Joo, O. S. Electrochemically deposited nanograin ruthenium oxide as a pseudocapacitive electrode. *Int. J. Electrochem. Sci.* (2007).
71. Zeng, Z., Zhou, H., Long, X., Guo, E. & Wang, X. Electrodeposition of hierarchical manganese oxide on metal nanoparticles decorated nanoporous gold with enhanced supercapacitor performance. *J. Alloys Compd.* (2015). doi:10.1016/j.jallcom.2015.01.240
72. Saravanakumar, B., Purushothaman, K. K. & Muralidharan, G. V₂O₅ / nitrogen enriched mesoporous carbon spheres nanocomposite as supercapacitor electrode. *Microporous Mesoporous Mater.* (2018). doi:10.1016/j.micromeso.2017.09.010
73. Antiohos, D., Romano, M., Chen, J. & Razal, M, J. Carbon Nanotubes for Energy Applications, Syntheses and Applications of Carbon Nanotubes and Their Composites. *IntechOpen.* (2013). DOI: 10.5772/51784
74. Bulakhe, R. N., Nguyen, V. H. & Shim, J. J. Layer-structured nanohybrid MoS₂@rGO on 3D nickel foam for high performance energy storage applications. *New J. Chem.* (2017). doi:10.1039/c6nj02590k
75. Thangappan, R. *et al.* Graphene decorated with MoS₂ nanosheets: A synergetic energy storage composite electrode for supercapacitor applications. *Dalt. Trans.* (2016). doi:10.1039/c5dt04832j
76. Vikraman, D. *et al.* One-pot facile methodology to synthesize MoS₂-graphene hybrid nanocomposites for supercapacitors with improved electrochemical capacitance. *Compos. Part B Eng.* (2019). doi:10.1016/j.compositesb.2018.12.143
77. Liu, Z., Qin, A., Yang, B., Wang, D. & Zhang, Z. Flower-like MoS₂ onto nitrogen-doped 3D graphene composite with active material for supercapacitor electrodes. *Mater. Lett.* (2019). doi:10.1016/j.matlet.2019.01.018
78. Masikhwa, T. M., Madito, M. J., Bello, A., Dangbegnon, J. K. & Manyala, N. High performance asymmetric supercapacitor based on molybdenum

- disulphide/graphene foam and activated carbon from expanded graphite. *J. Colloid Interface Sci.* (2017). doi:10.1016/j.jcis.2016.10.095
79. Zheng, S. *et al.* MoS₂ Nanosheet Arrays Rooted on Hollow rGO Spheres as Bifunctional Hydrogen Evolution Catalyst and Supercapacitor Electrode. *Nano-Micro Lett.* (2018). doi:10.1007/s40820-018-0215-3
 80. Da Silveira Firmiano, E. G. *et al.* Supercapacitor electrodes obtained by directly bonding 2D MoS₂ on reduced graphene oxide. *Adv. Energy Mater.* (2014). doi:10.1002/aenm.201301380
 81. Lamberti, A. Flexible supercapacitor electrodes based on MoS₂-intercalated rGO membranes on Ti mesh. *Mater. Sci. Semicond. Process.* (2018). doi:10.1016/j.mssp.2017.06.046
 82. Nandi, D. K. *et al.* Highly Uniform Atomic Layer-Deposited MoS₂ @3D-Ni-Foam: A Novel Approach to Prepare an Electrode for Supercapacitors. *ACS Appl. Mater. Interfaces* (2017). doi:10.1021/acsami.7b12248
 83. Xu, X. *et al.* Flexible symmetric supercapacitor with ultrahigh energy density based on NiS/MoS₂ @N-rGO hybrids electrode. *J. Colloid Interface Sci.* **543**, 147–155 (2019).
 84. Cocuzza, M. *et al.* High-Performing and Stable Wearable Supercapacitor Exploiting rGO Aerogel Decorated with Copper and Molybdenum Sulfides on Carbon Fibers. *ACS Appl. Energy Mater.* (2018). doi:10.1021/acsaem.8b00904
 85. Donarelli, M. & Ottaviano, L. 2D Materials for Gas Sensing Applications: A Review on Graphene Oxide, MoS₂, WS₂ and Phosphorene. *Sensors (Basel, Switzerland)* (2018). doi:10.3390/s18113638
 86. Arundel, A. V., Sterling, E. M., Biggin, J. H. & Sterling, T. D. Indirect health effects of relative humidity in indoor environments. *Environ. Health Perspect.* (1986).
 87. Mamishev, A. V., Sundara-Rajan, K., Yang, F., Du, Y. & Zahn, M. Interdigital sensors and transducers. in *Proceedings of the IEEE* (2004). doi:10.1109/JPROC.2004.826603
 88. Farahani, H., Wagiran, R. & Hamidon, M. N. Humidity sensors principle, mechanism, and fabrication technologies: A comprehensive review. *Sensors (Switzerland)* (2014). doi:10.3390/s140507881
 89. Kim, Y. H. *et al.* Ultrasensitive reversible oxygen sensing by using liquid-exfoliated MoS₂ nanoparticles. *J. Mater. Chem. A* (2016). doi:10.1039/c6ta01277a
 90. Lee, K., Gatensby, R., McEvoy, N., Hallam, T. & Duesberg, G. S. High-performance sensors based on molybdenum disulfide thin films. *Adv. Mater.* (2013). doi:10.1002/adma.201303230
 91. Li, Y. *et al.* MoS₂ nanoparticles grown on graphene: An advanced catalyst for the hydrogen evolution reaction. *J. Am. Chem. Soc.* (2011). doi:10.1021/ja201269b
 92. Du, B. *et al.* MoS₂-based all-fiber humidity sensor for monitoring human breath with fast response and recovery. *Sensors Actuators, B Chem.* (2017). doi:10.1016/j.snb.2017.04.193
 93. May, P., Khan, U., Hughes, J. M. & Coleman, J. N. Role of solubility parameters in understanding the steric stabilization of exfoliated two-dimensional nanosheets by adsorbed polymers. *J. Phys. Chem. C* (2012). doi:10.1021/jp302365w

94. El Garah, M. *et al.* MoS₂ nanosheets via electrochemical lithium-ion intercalation under ambient conditions. *FlatChem* (2018). doi:10.1016/j.flatc.2018.06.001
95. Y. Zhu, S. Murali, W. Cai, X. Li, J.W. Suk, J.R. Potts, R.S. Ruoff. Graphene and Graphene Oxide: Synthesis, Properties, and Applications. *Adv. Mater.* (2010). doi: 10.1002/adma.201001068
96. Stollenwerk, A. J. *et al.* Room Temperature Formation of Carbon Onions via Ultrasonic Agitation of MoS₂ in Isopropanol. *J. Nanosci. Nanotechnol.* (2017). doi:10.1166/jnn.2018.14707
97. Delgado, A. *et al.* Characterization of 2D MoS₂ and WS₂ Dispersed in Organic Solvents for Composite Applications. in *MRS Advances* (2016). doi:10.1557/adv.2016.531
98. Joseph, N., Muhammed Shafi, P. & Chandra Bose, A. Metallic 1T-MoS₂ with defect induced additional active edges for high performance supercapacitor application. *New J. Chem.* (2018). doi:10.1039/c8nj02087f
99. Li, X. *et al.* Co stabilized metallic 1T MoS₂ monolayers: Bottom-up synthesis and enhanced capacitance with ultra-long cycling stability. *Mater. Today Energy* (2018). doi:10.1016/j.mtener.2017.11.004
100. Forsberg, V. *et al.* Exfoliated MoS₂ in Water without Additives. *PLoS One* (2016). doi:10.1371/journal.pone.0154522
101. Shen, J. *et al.* Liquid Phase Exfoliation of Two-Dimensional Materials by Directly Probing and Matching Surface Tension Components. *Nano Lett.* (2015). doi:10.1021/acs.nanolett.5b01842
102. Bang, G. S. *et al.* Effective liquid-phase exfoliation and sodium ion battery application of MoS₂ nanosheets. *ACS Appl. Mater. Interfaces* (2014). doi:10.1021/am4060222
103. Ji, S. *et al.* Exfoliated MoS₂ nanosheets as efficient catalysts for electrochemical hydrogen evolution. *Electrochim. Acta* (2013). doi:10.1016/j.electacta.2013.07.094
104. Mahmood, Q. *et al.* Transition from Diffusion-Controlled Intercalation into Extrinsic Pseudocapacitive Charge Storage of MoS₂ by Nanoscale Heterostructuring. *Adv. Energy Mater.* (2016). doi:10.1002/aenm.201501115
105. Li, H. *et al.* From bulk to monolayer MoS₂: Evolution of Raman scattering. *Adv. Funct. Mater.* (2012). doi:10.1002/adfm.201102111
106. Sui, Z., Zhang, X., Lei, Y. & Luo, Y. Easy and green synthesis of reduced graphite oxide-based hydrogels. *Carbon N. Y.* (2011). doi:10.1016/j.carbon.2011.06.006
107. Glass, D. E. & Surya Prakash, G. K. Effect of pH on the Reduction of Graphene Oxide on its Structure and Oxygen Reduction Capabilities in the Alkaline Media. *Electroanalysis* (2018). doi:10.1002/elan.201800177
108. Lin, H. *et al.* Rapid and highly efficient chemical exfoliation of layered MoS₂ and WS₂. *J. Alloys Compd.* (2017). doi:10.1016/j.jallcom.2016.12.388
109. Huang, K. J., Zhang, J. Z., Shi, G. W. & Liu, Y. M. Hydrothermal synthesis of molybdenum disulfide nanosheets as supercapacitors electrode material. *Electrochim. Acta* (2014).

110. Roldán, S. *et al.* An approach to classification and capacitance expressions in electrochemical capacitors technology. *Phys. Chem. Chem. Phys.* (2015). doi:10.1039/c4cp05124f
111. Jiang, L. *et al.* Monolayer MoS₂-Graphene Hybrid Aerogels with Controllable Porosity for Lithium-Ion Batteries with High Reversible Capacity. *ACS Appl. Mater. Interfaces* (2016). doi:10.1021/acsami.5b10692
112. Saraf, M., Natarajan, K. & Mobin, S. M. Emerging Robust Heterostructure of MoS₂ -rGO for High-Performance Supercapacitors. *ACS Appl. Mater. Interfaces* (2018). doi:10.1021/acsami.8b04540
113. Gao, Y. P., Huang, K. J., Wu, X., Hou, Z. Q. & Liu, Y. Y. MoS₂ nanosheets assembling three-dimensional nanospheres for enhanced-performance supercapacitor. *J. Alloys Compd.* (2018). doi:10.1016/j.jallcom.2018.01.110
114. Huang, K. J. *et al.* Layered MoS₂ -graphene composites for supercapacitor applications with enhanced capacitive performance. *Int. J. Hydrogen Energy* (2013). doi:10.1016/j.ijhydene.2013.08.112
115. Zhang, L. & Shi, G. Preparation of highly conductive graphene hydrogels for fabricating supercapacitors with high rate capability. *J. Phys. Chem. C* (2011). doi:10.1021/jp204036a
116. Jung, S. M., Mafra, D. L., Lin, C. Te, Jung, H. Y. & Kong, J. Controlled porous structures of graphene aerogels and their effect on supercapacitor performance. *Nanoscale* (2015). doi:10.1039/c4nr07564a
117. Zhao, J. *et al.* Highly Sensitive MoS₂ Humidity Sensors Array for Noncontact Sensation. *Adv. Mater.* (2017). doi:10.1002/adma.201702076
118. Li, N., Chen, X. D., Chen, X. P., Ding, X. & Zhao, X. Ultra-high sensitivity humidity sensor based on MoS₂/Ag composite films. *IEEE Electron Device Lett.* (2017). doi:10.1109/LED.2017.2699332
119. Park, S. Y. *et al.* Highly selective and sensitive chemoresistive humidity sensors based on rGO/MoS₂ van der Waals composites. *J. Mater. Chem. A* (2018). doi:10.1039/c7ta11375g
120. Tan, Y. *et al.* The combinations of hollow MoS₂micro@nano-spheres: One-step synthesis, excellent photocatalytic and humidity sensing properties. *J. Mater. Chem. C* (2014). doi:10.1039/c4tc00423j